JPRS-JST-89-003
27 JANUARY 1989

FOREIGN BROADCAST INFORMATION SERVICE

JPRS Report

Science & Technology

Japan

19990211 084

DTIC QUALITY INSPECTED 3

DISTRIBUTION STATEMENT A
Approved for public release;
Distribution Unlimited

JPRS-JST-89-003

27 JANUARY 1989

SCIENCE & TECHNOLOGY

JAPAN

CONTENTS

TSC in Conducting Polymers

43067029 Tokyo THE TRANSACTIONS OF THE INSTITUTE OF ELECTRICAL ENGINEERS OF JAPAN in Japanese Jul 88 pp 287-292

[Article by Mitsuyoshi Onoda, member, Kiyoshi Amakawa, member, Department of Electrical Engineering, Himeji Institute of Technology, Hal Bon Gu, member, Department of Electrical Engineering, Faculty of Engineering, Osaka University, and Katsumi Yoshino, member, Department of Electronics, Faculty of Engineering, Osaka University]

[Excerpt] **1. Preface**

Previously, it was common sense to regard any polymer as an insulator. However, recently it has been learned that polymers with a highly developed conjugate system in their main molecular chains are highly electroconductive, and these polymers are drawing much attention as conducting polymers.[1] Although many conducting polymers themselves are insulators, the insulator-to-metal transition can be effected by doping with an appropriate material to realize high conductivity.[2].

The most representative conducting polymer is polyacetylene (PAc), whose electric, optical, and magnetic properties, as has been suggested, need to be explained by considering solitons and charged solitons in addition to ordinary electrons and positive holes.[3] On the other hand, polarons and bipolarons are considered more important than solitons and charged solitons for many conducting polymers including polythiophene and polypyrrol.[3]

Thus, even similar conjugate-type conducting polymers, with a slight difference in molecular structure, have vastly different properties. Charged solitons, polarons, and bipolarons represent a certain kind of deficiency in the undoped polymeric skeleton. One of the most effective methods to investigate deficiencies of polymers is the measurement of thermally-stimulated current (TSC). Thus far, the only example of TSC measurements for conducting polymers has been the report, on PAc, by Yoshino, et al.,[4] and this type of research has almost never been conducted.

This paper discusses TSC in poly (p-phenylenevinylene) (PPV), an alternate copolymer of acetylene and phenylene, and poly-chlorphenylacetylene (PCPA), a derivative of PAc, and the doping effects with iodine (I_2).

2. Samples and Experimental Methods

PPV films were prepared by the method of Murasa and others.[5] First, an aqueous solution of polymeric sulfonium salt was prepared by the condensation polymerization in an alkali solution of the monomer, p-xylylene-bis-(diethylsulfonium bromide). The resulting solution was purified by dialysis and films of polymeric sulfonium salt were obtained by casting the solution. The films were heat-treated for approximately 1 hour at 300°C at a reduced pressure to remove the sulfonium salt to obtain PPV films.

PCPA films were prepared by casting from a suitable catalyst such as chloroform, a solution of PCPA powder, which had been polymerized from chlorphenylacetylene gas with an ordinary Ziegler catalyst.[6]

The molecular structures of PPV and PCPA are shown in Figure 1. The I_2 doping of PPV was accomplished by exposing PPV films to I_2 atmosphere in a 40°C constant temperature bath for a specified time. To I-$_2$-dope PCPA, it was redissolved in chloroform with I_2 and films were cast from the solution to obtain I_2-doped PCPA films. The quantity of doped I_2 was determined by measuring the amount of mixed I_2.

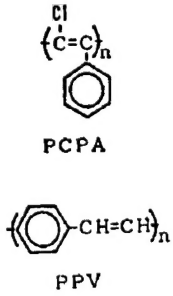

Figure 1. Molecular Structures of Polychlorophenylacetylene (PCPA) and Poly(p-phenylene vinylene) PPV)

The measurement of TSC was done as follows: After applying DC voltage for 1 hour at 30°C, the temperature was quickly lowered to -70°C while still applying the voltage. At the low temperature the electrodes were shorted to let the discharge current stabilize for 10 minutes. Then, the current through the external circuit was measured while the temperature was being raised at a speed, β, of 2°C per minute. The experiments were conducted in a vacuum of approximately 1 x 10^{-3} Pa, and a multichannel potentiometer (Keithley 610C) was used to determine electric conductivity. Also, gold was vacuum-vapor-deposited on the main electrodes of 6 mm in diameter. The direction of TSC was set positive in the direction of ordinary discharge current, i.e. the opposite of the current direction at sample charging.

3. Experimental Results and Discussion

(3.1) TSCs of PPV

It has been known that the thermal decomposition of polymeric sulfonium salt begins at about 90°C and continues through 300°C. Figure 2 shows the TSC values observed for PPV which was heat-treated at 300°C after impressing various strengths of the poling field. Within the temperature range used in the experiments, TSC is observed in the direction of ordinary discharge currents and the peaks are seen around 60°C. As the poling field increases, TSC generally show higher values. Also an activation energy of 0.5 eV was obtained from the portions of curves where TSC begins rising.

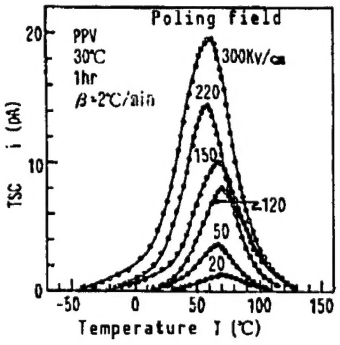

Figure 2. Dependence of TSC Spectra for Undoped PPV on Poling Fields

In Figures 3(a) and (b) TSC is shown as observed after the impression of a poling field of 100 kV/cm for polymer samples which were I_2-doped for various time periods. The characteristics of TSC are shown when the doping time is relatively short as in Figure 3(a); those for longer doping times are shown in Figure 3(b). In Figure 3(a), the TSC peak for undoped PPV is seen in the vicinity of 60°C and, as the doping time increases, TSC values generally become greater. Also, the temperature of each peak shifts toward lower temperatures, as the doping time increases. (Hereafter, this peak will be called P_1 peak.) As the doping time further increases, as shown in Figure 3(b), the P_1 peak passes its maximum at about 40 minutes of doping time, and thereafter gradually becomes smaller. Also, the peak temperature shifts toward the low side. Furthermore, new peaks are observed at about 50°C and their magnitudes increase gradually with the doping time. (Hereafter, this peak will be called P_2 peak.) The measurements of TSC for I_2-doped PPV were repeated three times for the same sample. The measurements were repeated as the temperature was elevated to 100°C with relatively good reproducibility among three readings. However, when the temperature exceeds 100°C, TSC readings in general decrease gradually each time and reproducibility could not be observed. The reason for this is presumably the escape of I_2 at about 100°C. Also, the TSC for the PPV samples with the doping time of 180 and 300 minutes, respectively, after showing their P_1 and P_2 peaks, as shown in Figure 3(b), at about 100°C suddenly began rising and peaked at around 130°C. Furthermore, when the identically I_2-doped PPV

without impressing a poling field was heated in a short-circuited state, currents suddenly began to flow around 100°C and again peaked around 130°C. Therefore, the TSC spectra for the temperature region of 100°C and above for the PPVs with the doping time of 180 and 300 minutes, as shown in Figure 3(b), were drawn after correcting for the current component due solely to the above-mentioned temperature rise. When the doping time exceeded 300 minutes, the current component due only to temperature rise became more appreciable, and the temperature for the occurrence of the component shifted toward the low side, so it was impossible to separate the P_2 peak from the component.

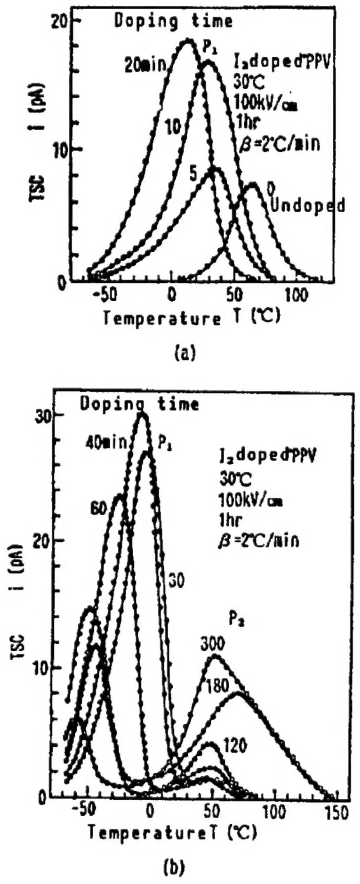

Figure 3. Dependence of TSC Spectra for I_2-Doped PPV on Doping Times

From the experimental results shown in Figure 3, the activation energies for P_1 and P_2 peaks, current values at peaks, and peak temperatures were obtained and they were plotted against the doping time as in Figure 4. In Figure 4, the activation energy of undoped PPV is shown to be about 0.5 eV, but the activation energy of the P_1 peaks for I_2-doped PPV decreases and remains at about 0.2 eV regardless of the doping time. The peak temperature for undoped PPV is in the vicinity of 60°C, but the peak temperatures for doped PPV shifts lower as the I_2 doping time becomes longer, and appears to show the saturation tendency at about -60°C. The P_1 peak currents, as shown in

the middle graph of Figure 4, initially show a rapid increase with the doping time, reach a maximum at about 40 minutes of doping time, and thereafter gradually decrease. Considering that the activation energy of undoped PPV is about 0.5 eV, and that for I_2-doped polymer drops to about 0.2 eV, and that the trap depth has apparently decreased, it is plausible that, as the doping time becomes longer and the I_2-doping quantity increases, the conductance between iodine molecules governs and it is difficult to trap carriers. On the other hand, P_2 peaks are observed with the doping time of about 30 minutes or longer, and the peak current value gradually increases, with the doping time. In addition, regardless of the doping time, the peak temperatures are in the neighborhood of 50°C and the activation energy is about 0.4 eV. It is clear from the above that TSCs for I_2-doped PPVs undergo extremely complicated changes.

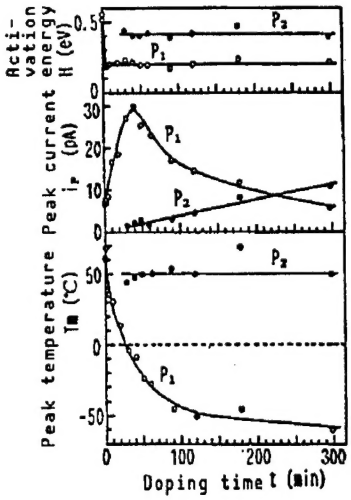

Figure 4. Relationships Among the Activation Energies of the TSC Peak, the Peak Values of the TSC and Its Appearance Temperatures Which Were Derived From the Data in Figure 3 and Doping Times

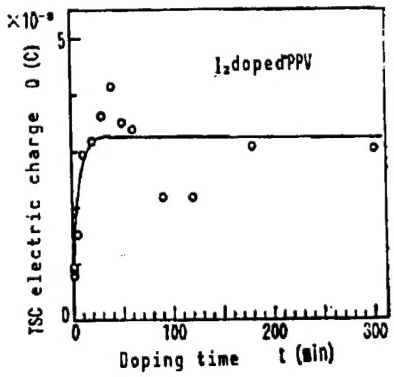

Figure 5. Relation Between the Electric Charge Calculated From the TSC Peak Area in Figure 3 and Doping Times

The PSC peak areas were obtained from the Figure 3 experiment to calculate the electric charges which are plotted against the doping time in Figure 5. It shows that when the doping time exceeds about 10 minutes the electric charge is saturated at about 3 x 10^{-8} (C).

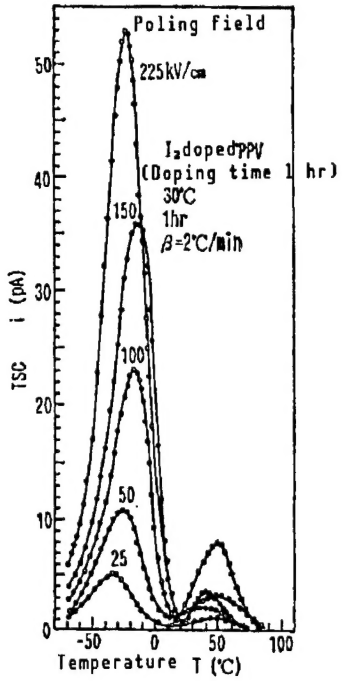

Figure 6. Dependence of TSC Spectra for I_2-Doped PPV on Poling Fields

Figure 6 shows TSC for an I_2-doped (1 hour) PPV after impressing various strengths of poling field. The P_1 and P_2 peaks are seen at -20°C and 50°C, respectively, and, as the poling field intensifies, the TSC values as a whole become larger. In particular, the change at about the peak at -20°C is large.

Figure 7 represents the relationship between the electric charge and the poling field which is calculated from the TSC peak areas obtained from the experiments in Figures 2 and 6. According to the graph, the charge increases with the poling field almost in a straight line, and the charge for the I_2-doped PPV is nearly three times that for the undoped PPV.

So far, TSC and the I-$_2$-doping effects for PPV have been discussed. Although it is not possible to determine definitely the source for the trap from the above-discussed experimental results, it is well known that I_2 efficiently catches electrons in many inductors.[7] Based on this fact, it is surmised that the P_1 peaks observed in the low temperature side for I_2-doped PPVs are caused by the electron trap formed by the effect of the iodine molecules of the dope. In other words, the P_1 peaks, whose activation energies are about 0.2 eV and almost constant regardless of any increase in the I_2-doping quantity, can be considered to be a defect created by I_2-doping.

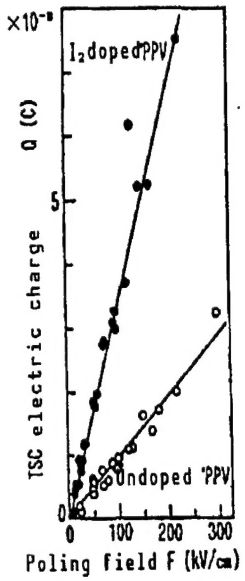

Figure 7. Relation Between the Electric Charge Calculated From the TSC Peak Area in Figure 2 and Poling Fields

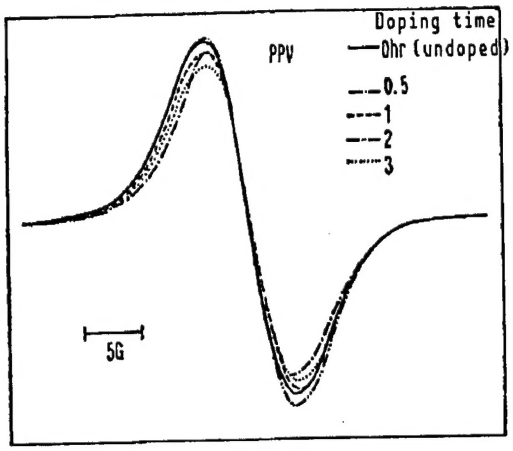

Figure 8. ESR Spectra for Undoped and I_2-Doped PPV

On the other hand, the activation energies for the P_2 peaks, which appear in the high temperature region for I_2-doped PPVs, do not change significantly with the increase in I_2 quantity and stay at about 0.4 eV which is not much different from that for the undoped PPV. These P_2 peaks emerge in the almost same temperature region as the TSC peak for the undoped PPV.

Figure 8 shows the ESR (JES FE-3XG by Nippon Electronic Co., Ltd.) spectra of PPVs as measured with varied I_2-doping time. The ESR signals of I_2-doped PPVs are very small and as broad as 8 G regardless of the doping time. The spin density of about 5×10^{17} (spins/g) is indicated, showing no meaningful difference from the ESR signal for the undoped PPV.

Generally speaking, when conducting polymers are doped with an appropriate substance, an insulator-to-metal transition occurs, the ESR signal peak widths narrow and the spin density increases.[8]

In the present experiments, ESR measurements were carried out at room temperature (about 20°C) with I_2-doped PPV sealed in a vacuum. The escape of I_2 was thought to occur from about 100°C, as judged from the TSC measurements. Based on this, the reason for the ESR signals for I_2-doped PPVs being about the same as the signals for undoped PPV was probably that the ESR signals did not change appreciably by doping because the amount of doping was small. Figure 8 indicates the relatively high spin densities of the PPV, hinting at the possible existence of localized sub-levels. Considering the PPV synthesis methods, some of the impurities, which could

not be removed by heat treatment, are thought to remain in PPV to form relatively deep sub-levels. Perhaps it can be reasoned that slight amounts of Br_2 and SO_3, which had been produced by the decomposition of the polymeric sulfonium salt, were accidentally doped into PPV to form a low density polaron state. Therefore, the ESR signals obtained in the experiments are thought to have been caused by the defects originally existing in PPV. From these experimental results, it is surmised that the TSC peaks of undoped PPV and the P_2 peaks of I_2-doped PPVs are centered around the localized defects which were in PPV to begin with.

(3.2) TSC of PCPA

Recently, Yoshino, et al., have been determining TSCs for PAc, oxygen-doped PAc, and γ-irradiated PAc. In the present experiment, TSC was determined for PCPA, a substitution derivative of PAc, to study how properties change by the substitution.

TCSs were observed for PCPAs, which had been doped with varying amounts of I_2, after polarizing at 300 kV/cm. Results are shown in Figure 9. In the temperature region of these experiments, TSCs were observed in the direction of normal discharge currents, and the main peaks for both undoped and I_2-doped PCPAs appear in the vicinity of 50°C. (Hereafter, these peaks will be called P_1 peaks.) Other faint peaks are observed around -40°C. (Hereafter, these peaks will be called P_2 peaks.) As the quantity of I_2 doping increases, overall P_1 peaks move to a higher level and the peak temperatures tend to shift only slightly toward the low side. However, P_2 peaks remain at the almost same level regardless of the I_2-doping quantity, and their temperatures show practically no shifting.

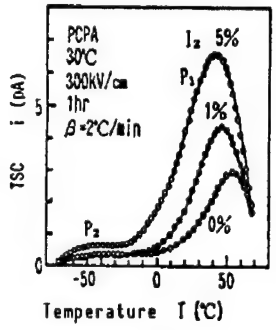

Figure 9. TSC Spectra for Undoped and I_2-Doped PCPA Polarized at 300 kV/cm

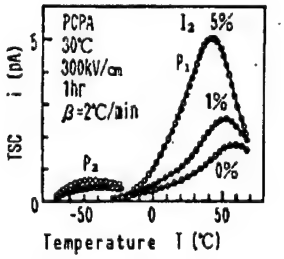

Figure 10. Thermal Cleaning for TSC Spectra in Figure 9

The P_1 and P_2 peaks obtained in Figure 9 are separated by the thermal cleaning method, and results are given in Figure 10. As clearly seen by comparing with the experimental results shown in Figure 9, for a given sample, two P_2 peaks (Figure 9 and Figure 10) indicate about the same magnitude, but the P_1 peaks in Figure 10 appear to shrink slightly from the corresponding peaks in Figure 9. It is not clear at this time why the P_1 peaks are lowered by the thermal cleaning, but it is likely that TSC is influenced by the heat treatment effect and the escape of I_2 caused by the

thermal cleaning. Therefore, the evaluation of P_1 peaks is not necessarily easy. The activation energies for P_1 and P_2 peaks were obtained from the curves' initial rising portions in Figure 10. They were approximately 0.4 and 0.2 eV, respectively, and were found to be almost constant regardless of the quantity of I_2.

According to the report by Yoshino, et al.,[4] who evaluated the depth of the trap in PAc from the TSC measurement, the electron trap formed by the effects of the defects originally existing in PAc and of the adsorbed oxygen are localization-centered. Also, according to the report,[4] although the TSC characteristics are not clear for I_2-doped PAc, the P_1 and P_2 peaks corresponding to the TSC spectra of PCPA, as shown in Figure 9, are not observed with PAc.

It is impossible to determine definitely the source of the trap for each peak based on the above-discussed experimental results. However, because the magnitude of the P_1 peak increases with the I_2 quantity and decreases slightly with thermal cleaning, it is somewhat unreasonable to suggest that the peak is caused by depolarization due to the substitution radical of PCPA. On the other hand, the P_2 peak can be considered to be caused by the depolarization due to the substitution radical of PCPA, because the peak's magnitude does not change with the I_2 quantity or with thermal cleaning.

The activation energy of the P_1 peak changes little and remains at approximately 0.4 eV even with the increase of I_2 quantity. Furthermore, the P_1 peak for undoped PCPA occurs at about 50°C. Thus, it can be deduced that the localization centers for the P_1 peak for PCPA are based on the defects originally existing in the polymer, similar to the case of PPV. However, as previously discussed regarding the TSC characteristics of PPV, I_2 effectively captures electrons in many inductors. It can be inferred then, that the P_1 peak is also based on the electron trap formed by the effect of doped I_2 molecules. Therefore, it is possible that defects are formed in I_2-doped PCPA, similar to the case of undoped PCPA. At the present stage, it is impossible to decide definitely whether the localization centers for the P_1 peak for I_2-doped PCPA are due to the defects originally existing in PCPA or due to the defects formed by I_2 doping.

The results of TSC microscopes for samples of PPV and PCPA have been presented. It is evident that the TSC measurement is effective in the study of conducting polymers.

4. Summary

The depth of trap and the localization center were evaluated for PVP and PCPA by measuring TSC and the effects of I_2 doping on TSC. The TSC peak for undoped PPV was observed in the vicinity of 60°C, and it is deduced that he localization centers are due to the defects originally existing in PPV. The trap depth was evaluated as approximately 0.5 eV. Two peaks of P_1 and P_2 were observed in the TSC spectra of I_2-doped PPV. The P_1 peak is thought to be caused by the electron trap formed by I_2 doping, and the depth of the trap was found to be approximately 0.2 eV. The P_2 peak was observed in the temperature region similar to that in which the TSC peak for undoped PPV

appeared, and the trap depth was also about the same as that for undoped PPV. Thus, for the P_2 peak, the localization center is considered to be based on the defects originally existing in PPV.

The TSC spectra for undoped PCPA and I_2-doped PCPA show two peaks of P_2 and P_1 around -40°C and 50°C, respectively. For the P_1 and P_2 peaks, the activation energy was determined to be approximately 0.4 and 0.2 eV, respectively, regardless of the quantity of I_2. The P_2 peak, it is thought is caused by depolarization due to the substitution radical of PCPA.

With the P_1 peak, the localization centers are caused by the defects originally existing in PCPA. However, because the I_2 doping of PCPA causes the same defects as that of undoped PCPA, and because the defects can become localization centers, it is impossible definitely to determine, at the present stage, whether the localization centers for the P_1 peak of I_2-doped PCPA are due to the defects originally existing in PCPA or due to the defects formed by I_2 doping.

This research was partially subsidized by the science research fund of the Ministry of Education.

(Received 24 November 1987)

References

1. Sakabe, chief editor, "Conducting Polymeric Materials, 1983, C.M.C., p 49.

2. Ibid., p 59.

3. Ibid., p 64.

4. K. Yoshino, T. Sakai, Y. Yamamoto, and Y. Inuishi, "Thermally Stimulated Current in Polyacetylene," JPN. J. APPL. PHYS., Vol 20, 1981, p 867.

5. Murase, Onishi, Noguchi, and Hirooka, "Conducting Polyphenylenevinylene Films," Insulator Research Data, Institute of Electrical Engineers of Japan, EIM-85-72, 1985.

6. M. Onoda, K. Amakawa, H.B. Gu, and K. Yoshino, "Thermally-Stimulated Current Measurements and Localized States in Polychlorophenylacetylene," JPN. J. APPL. PHYS., Vol 25, 1986, p 818.

7. Onoda, Nakayama, and Amakawa, "Reverse TSC for Iodine-Doped Low Density Polyethylene," J. OF APPLIED PHYSICS, Vol 56, 1987, p 657.

8. Yoshino, Hayashi, Takiguchi, Kanefuji, and Shiraishi, "Electrochemical Doping of Multi-Element Five-Member Ring-Type Conducting Polymers and Their Electric and Optical Properties," The Transactions of the Institute of Electrical Engineers of Japan, Vol 106-A, No 4, 1986, p 171.

45-m Radio Telescope, Deep-Space Exploration Antenna Developed

43062581 Tokyo KEISOKU TO SEIGYO in Japanese Jul 88 pp 88-89

[Article in "Product Introduction" feature pages, by Communications Equipment Manufacturing Center, Mitsubishi Electric Co.]

[Text] 1. Introduction

The 45-m radio telescope has already been installed in the Nobeyama Cosmic Radio Wave Observatory of the National Astronimal Observatory for the observation of space using millimeter waves. This telescope features a high millimeter-wave condensing ability and high resolution; many astronomers from all over the world share in using this telescope, which has contributed to the discovery of new interplanetary matter and rotating gas clouds in protoplanets. The mirror accuracy (condensation) and directivity of the 45-m telescope is being improved. It is also expected to be used in VLBI (Very Long Baseline Interferometry) on a global scale or in conjunction with space-based VLBI.

A large antenna was built at the Usuda Space Observatory in Naganoken for deep-space exploration. It is a 64-m antenna, and is for tracking deep-space probes at distances of up to 220 million kilometers in order to acquire observation data from them and control them. For example, this antenna was used in observing Halley's comet, which returned to near the Sun after 76 years, by tracking and controlling two probes "Sikigake" and "Suisei". In the future, it will be modified to be compatible to both S/X bands and multi-band operations so that it can be used in research fields other than deep-space exploration, such as VLBI, and in international cooperation with NASA.

2. Main Features and Performance

Both the 45-m radio telescope and deep-space antenna must have very accurate directivity to detect the objects and space probes precisely. The factors that can introduce errors affecting directivity include mechanical setting errors related to verticality and orthogonality, angle detection error, and deformation errors due to the antenna's own weight and wind pressure. The radio telescope and antenna use the following techniques to improve accuracy and counteract these error factors.

(1) Mechanical errors that tend to be repeated are corrected based on current source tracking data (instrumental error correction).

(2) The antenna main reflector is designed to be homologous, and focusing errors due to its own weight are corrected by the sub-reflector drive.

(3) The direction of the antenna main reflector is controlled by referring to a master collimator installed on a collimator tower which is provided separately from the antenna.

(4) For improved angle detection accuracy, the master collimator uses a multi-pole resolver directly coupled with the shaft.

(5) Errors due to external disturbances are reduced by reinforcing the rigidity of the mechanism and widening the servo range.

Table 1 shows the major capabilities of the 45-m radio telescope, and Table 2 shows deep-space exploration antenna.

Table 1. Main Performance of 45-m Radio Telescope

	Item		Specifications	Remark
General	Type		Cassegrain antenna	
	Antenna diameter		45-m	Sub-reflector diameter 3.75 m
	Feed system		Reflector type focusing beam feed	
	Mount		AZ-EL mount	The 2 axes are crossing
	Drive system	AZ	Rail-wheel anti-backlash type	DC motors 22 kW x 2
		EL	3-sector gear, 4-pinion anti-backlash type	DC motors 11 kW x 4
	Tracking system		- Programmed - Manual	
Mechanical	Main reflector surface accuracy		0.16 mm rms (actual measurement)	Overall, total elevation angle
	Main reflector drive range	AZ	$\pm 270^{o}$ (with respect to south)	Mechanical limit
		EL	9 to 93^{o}	

Electro-mechanical	Directivity accuracy	Less than ±5"	- Night wind velocity less than 7 m/s
	Max. drive speed	0.5/s or more	With both axes
	Max. drive acceleration	0.5 s^2 or more	

Table 2. Main Performance of Deep-Space Exploration Antenna

	Item		Specifications	Remark
General	Type		Cassegrain antenna with shaped reflector	
	Reflector diameter		64 m	Sub-reflector diameter 6 m
	Feed system		Reflector type focusing beam feed	SX shared use possible in future
	Mount		AZ-EL mount	The 2 axes cross
	Drive system	AZ	Rail-wheel anti-backlash type	DC motors 55 kW x 2
		EL	2-sector gear, 4-pinion anti-backlash type	DC motors 30 kW x 4
	Tracking system		- Programmed (Truck slave) - Programmed scan - Manual - Mono-pulse auto-tracking	
Mechanical	Main reflector surface accuracy		1.5 mm rms (actual measurement)	Overall, total elevation angle
	Main reflector drive range	AZ	±270° (with respect to south)	Mechanical limit
		EL	5 to 92°	
Electro-mechanical	Directivity accuracy (Reproducibility)			

Stationary accuracy	Less than ±5" (Less than 0.003° rms in X band)	- Night wind velocity less than 8 m/s
Dynamic accuracy	C + C : C - 0, C = 1.4 or less	
Max. drive speed	0.5/s or more	)
Max. drive acceleration	0.5 s^2 or more	) With both axes

3. Summary of Configuration and Operation

As shown in Figure 1, the deep-space exploration antenna consists of a reflector block, focusing beam feeder block, rotation structure blocks, drive block, master collimator and drive controller unit. The drive controller unit is composed of the main reflector drive controller, master collimator drive controller, sub-reflector drive controller, instrumental error corrector and antenna control console.

3.1 Main reflector drive controller

The AZ (azimuth) of the main reflector is controlled by the anti-backlash drive of two DC motors installed on two of the sixteen trucks, and the EL (elevation angle) is controlled by anti-backlash drive of four DC motors, which are installed as pairs on each of the two sector gears facing each other across the master collimator. The main reflector follows the master collimator for the antenna direction control based on a program or other means.

3.2 Master collimator drive controller

For very accurate antenna angle detection, an optical master collimator is installed at the point where the AZ and EL axes cross on an independent tower, away from the antenna. The collimator tracks the reflection from the mirror which is set to the centering position, and the collimator rotation angle is detected by a multi-pole resolver.

3.3 Sub-reflector drive controller

An antenna should have a high mirror accuracy in order to obtain high condensation. These antennas are built using a homologous design so that the mirror surface maintains a parabolic curve even when deformed due to its own weight, important with such a large antenna. As the homologous design results in the deviation of the main reflector focusing position following the rotation of the elevation angle, focusing is adjusted under the control of the sub-reflector.

3.4 Instrumental Error Corrector

The main features of this are as follows.

(1) Correction of instrumental errors inherent in the antenna

This feature corrects mechanical errors which are inherent in the antenna, that tend to be reproduced repeatedly. These errors occur due to problems in verticality, orthogonality between the AZ and EL axes, orthogonality between the EL and beam axes, deformation due to the antenna's own weight and reference angle errors. Correction values are obtained by tracking the radio wave source.

(2) Correction of homologous deformations of main reflector

To correct the deformation of the main reflector due to the antenna's own weight, the position of the sub-reflector is calculated as a function of the EL angle of the main reflector. The deviation in the direction angle is corrected as an instrumental error caused by deformation due to its own weight.

Figure 1. Construction of Deep-Space Exploration Antenna

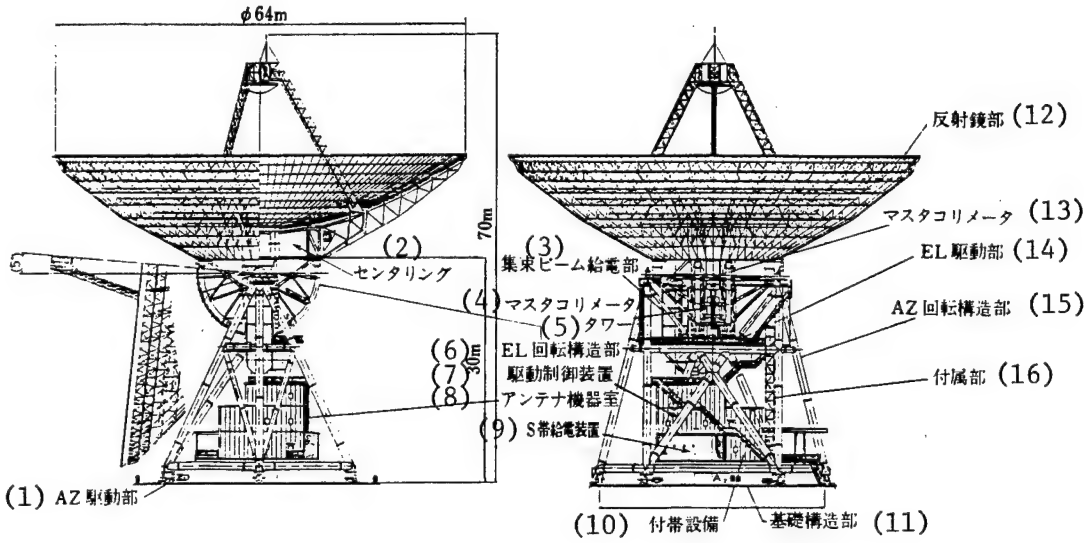

Key:

1. AZ driver
2. Centering unit
3. Focusing beam feeder block
4. Master collimator
5. Tower
6. EL rotation structure block
7. Drive controller unit
8. Antenna equipment room
9. S band feed unit
10. Miscellaneous equipment
11. Foundation structure
12. Reflector block
13. Master collimator
14. EL driver
15. AZ rotation structure block
16. Additional equipment

4. Conclusion

In closing, we expressed our gratitude to Professor Morimoto of the National Astronomical Observatory, Professor Hayashi of the Institute of Space and Astronautical Science]ISAS] and others concerned, for their advice and guidance in developing and manufacturing this equipment.

Mid-Term Report on Fifth Generation R&D

43067613a Tokyo JECC NEWS in Japanese 1 Jul 88 pp 4-5

[Text] The New Generation Computer Technology Development Organization (ICOT) held its "Sixth Symposium on the Fifth Generation Computer" at the Kudan Kaikan (Hall), Kudanshita, Tokyo, 31 May to 1 June, to report the status of research and development and to demonstrate the sequential inference machine (PSI: personal sequential inference machine).

The fifth generation computer is expected to eliminate some restrictions encountered in conventional computer technologies and to meet high-performance information processing needs in the 1990s, efficiently implementing knowledge information processing through innovative ideas and novel theories and technologies.

ICOT, set up in April 1982 for the R&D of this computer, has a 10-year research and development plan consisting of a 3-year basic technology development plan, 4-year experimental small-scale subsystems development plan, and 3-year prototype system development plan (Figure 1).

The functions of the fifth generation computer are classified into the problem-solving/inference function, knowledge base management function, and intellectual interface function. ICOT intends to develop specific software and hardware systems for individual functions and to implement them based on logic programming and VLSI technology.

This is the 7th year of the overall plan and the last year of the mid-term plan, and has already witnessed practical results, including PSIs, in respective developmental fields. In fact, 7 PSIs were used to demonstrate 14 systems at the symposium, attracting the participants' attention.

Last year's results were reported at the symposium. Last year was the 3d year of the mid-term 4-year plan mainly intended to develop experimental small-scale subsystems, and provided trial debugging of software and the trial production of partial hardware systems for each of the following four systems: 1) inference subsystem, 2) knowledge base subsystem, 3) basic software system, and 4) development support system. The four systems are systematically described below and, on them, ICOT is accumulating fruitful achievements.

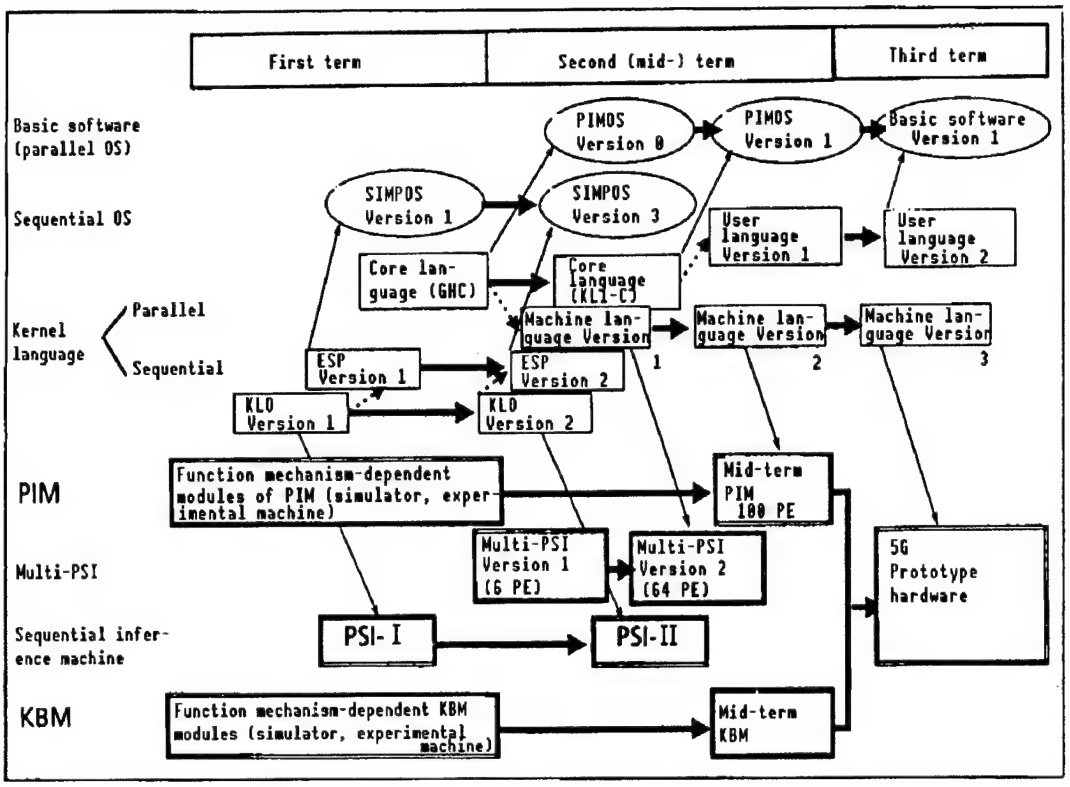

Figure 1. Flowchart of Hardware/Software Research and Development

1. Hardware system

    a. Inference subsystem
    b. Knowledge base subsystem

2. Basic software system

3. Development support system

The current status of these systems will be explained.

Hardware System

During the mid-term, the research and development of a hardware system has been carried out, based on the functional mechanism R&D for the inference subsystem, the R&D of such mechanisms as the knowledge base machine-related database mechanism, and the R&D of the sequential inference machine and, using the specifications of the parallel-type kernel language version 1 (KL1) as a guideline, all of which were implemented or designed during the first term.

A hardware R&D objective during the mid-term is to establish an inference subsystem machine architecture provided with a high-performance parallel

processing capability and a parallel machine architecture for a knowledge base subsystem. In other words, the objective is to pursue a general-purpose machine architecture particularly suitable for inference and knowledge base processing and serving as the core of the knowledge information processing software system.

Inference Subsystem

The mid-term R&D of the inference subsystem is intended to define the architecture of a parallel inference machine, consisting of as many as 100 element processors, and to experimentally manufacture hardware in order to conform its operation.

1. Improvement and expansion of machine language in parallel inference machine kernel language

Kernel language version 1 (KL1) is a GHC-based parallel logic language. The year before last the design specifications of KL1's machine language were completed, and an experiment using a control software was carried out last year. The experiment shows that KL1 consumes memory at a very high speed, and a batch-type garbage collection (GC) may occur to significantly reduce the processing speed unless some actions are taken.

If, during the execution of KL1, the guard section attempts to implement a calling variable, or the execution of a built-in predicate fails, the attempt to select the clause will fail and the execution of the next clause will begin.

Therefore, a technique to efficiently implement Kl1 on the parallel inference machine has been studied, and KL1's machine language has been improved and expanded. As a result, machine language instruction sets incorporating the GC method and closed indexing technique have been designed.

2. Parallel inference machine/hardware

The pilot model hardware shown in Figure 2 was designed based on continued study of the parallel inference machine architecture.

The parallel inference machine (PIM) consists of 128 processors coupled in a two-level hierarchy--some 8 element processors (PE) are tightly coupled by a shared bus to form a subsystem called a cluster, and 16 clusters are loosely coupled by a hyper-cube structure network to form the entire system. In addition, the main memory (shared memory) shared by eight PEs is also connected to the shared bus in a cluster.

The parallel inference machine itself has no I/O device, but a separate front end machine (FEP) handles the functions of user terminals, disks, and LAN interfaces. A small PSI is used for the FEP (Figure 3).

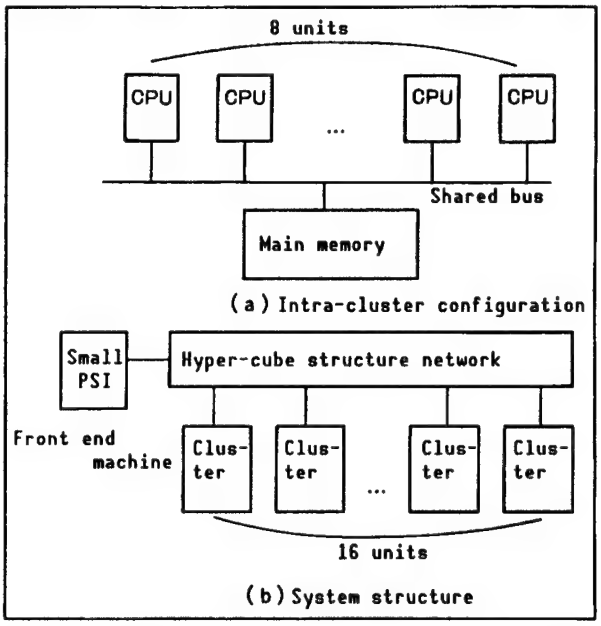

Figure 2. PIM Hardware System Structure

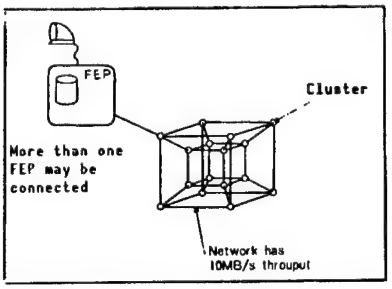

Figure 3. PIM System Structure

3. Parallel processing method for kernel language version 1

In order for the parallel inference machine, PIM, with the hardware structure shown in Figures 2 and 3, to have efficient processing as well as hardware, it is important to:

- Provide a sufficiently high speed to important processors (PEs)
- Improve interprocessor communications efficiency
- Distribute load appropriately

Accordingly, a method to implement the basic performance of KL1 on PEs has been designed, including a garbage collection and memory management method, to enhance memory usage efficiency and internal data representation, as well as the suspension implementation method. Another valuable design includes the efficient switching of PE processing and improved efficiency of network communications.

4. Trial production and evaluation of control software

In order to complete the KL1 processing method and detailed design of the architecture for the parallel inference machine, a pseudo-parallel processing system trial manufactured the previous year was expanded, and a parallel experiment processing system was trial manufactured for the experimental evaluation of technical elements.

Evaluation categories using the control software include:

- Evaluation of a parallel cache facility
- Evaluation using a parallel processing system
- Evaluation of MRB-GC

5. Detailed design of component modules

The research and development of PIM component modules is intended to achieve familiarization with a parallel execution machine, parallel execution method, and load distribution facility for the parallel inference machine. The detailed design and partial trial manufacture of three pilot modules--the data flow-type, reduction-type, and goal-rewriting type--were attempted last year.

6. Trial manufacture of a parallel hardware simulator

A parallel hardware simulator was trial manufactured to materialize KL1's parallel processing design and to support the development of parallel software systems, such as an operating system.

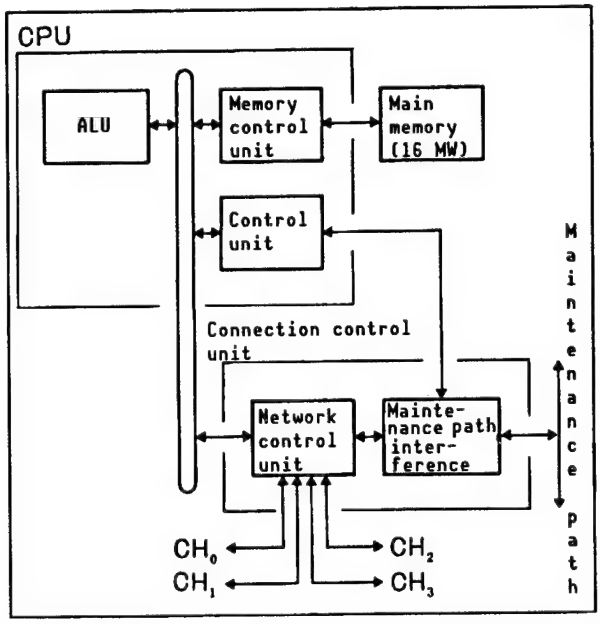

Figure 4. Element Processor Configuration

The parallel hardware simulator is such that the CPU of a small PSI, which is a sequential inference machine, is partially improved to form an element processor, with up to 64 of them coupled via a connection network. The element processor consists of the main memory, CPU, and connection control unit, as shown in Figure 4.

Knowledge Base Subsystem

The mid-term R&D objective of the knowledge base subsystem is to determine a technique to implement a knowledge operation mechanism required by a knowledge base machine, establish parallel architecture for the knowledge base machine, and trial manufacture the hardware.

1. Knowledge base parallel control mechanism

Last year, an experimental hardware machine and knowledge base parallel operation software were used to simulate the unified retrieval operation and to evaluate a parallel processing method. In addition, part of the knowledge base parallel operation software was trial manufactured.

In terms of an inference machine interface, the sequential inference machine PSI was interfaced with the knowledge base machine experimental hardware machine, the memory of the experimental machine was expanded, and a knowledge base operation engine was trial manufactured.

2. Distributed knowledge base control mechanism

Software was trial manufactured based on the detailed design implemented the previous year, and part of the software configuration was modified for more efficient knowledge processing and management. The detailed design and partial trial manufacture of a knowledge operation processing module experimental system, hardware system to supplement the distributed knowledge base machine experimental system PHI, were attempted.

3. Knowledge base constructing mechanism

Since a knowledge base application program processes enormous amounts of knowledge elements, names identifying those knowledge elements are difficult to manage and the same name might be assigned to different knowledge elements. To solve this problem, the multiple name space (package) was introduced and, with the use of multiple packages, different knowledge elements could have the same name providing they were in different packages.

4. Study of knowledge expression in the knowledge base subsystem

Parallel problem solving functions for solving large-scale artificial intelligence application problems efficiently on the parallel inference machine, PIM, as well as the knowledge retrieval function, were studied in detail.

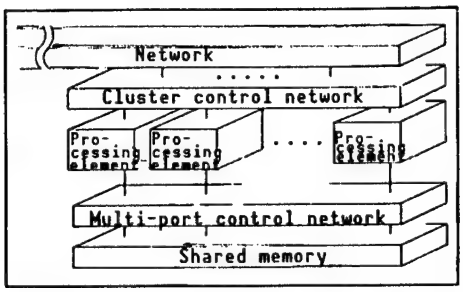

Figure 5. Conceptual Diagram of Knowledge Base Cluster Architecture

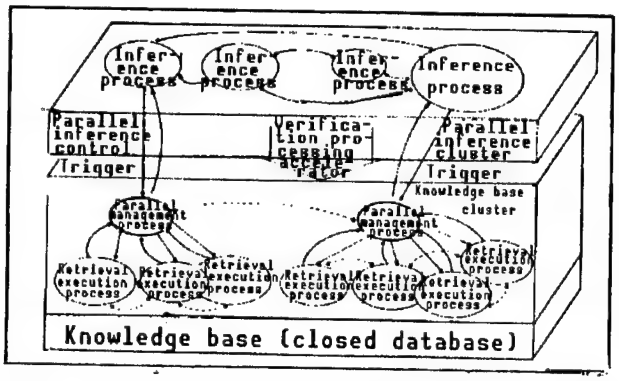

Figure 6. Process Configuration Concept Within Knowledge Base Cluster

Basic Software System

The research and development of the mid-term basic software system includes the expansion of the kernel language version 1, based on the results of the first-term basic technology development, the R&D of new software technologies such as parallel processing, based parallel inference control, the evaluation of elemental technologies developed during the first term, and trial manufacture of a more sophisticated system, all of which will join to form kernel language version 2.

In addition, basic studies will be made of high level inference functions and distributed knowledge base management intended for use in a joint problem solving system, which is the final target of the basic software system.

In the mid-term plan, the R&D of basic software is being promoted along the following six R&D themes:

- Fifth generation (5G) kernel language
- Problem solving/inference software module
- Knowledge base management software module
- Intelligent base management software module
- Intelligent programming/software module
- Basic software verification system

1. 5G kernel language

Kernel language version 1 (KL1) and version 2 (KL2) are being studied and developed.

KL1 is intended to expand language specifications, accelerate processing, implement processing in a parallel execution environment, and rearrange the programming system.

KL2 is intended to design language specifications with emphasis on knowledge representation functions, and identify and determine, based on the results of specification use, hardware support functions aimed at higher speed.

2. Problem solving/inference software module

The module is meant to develop a cooperative problem solving system and, therefore, to determine a problem solving implementation technique to support the system in a parallel environment. To attain these targets, parallel features covering a wide range of levels, from system programming to application levels, are being studied.

3. Knowledge base management software module

This theme is intended to set up the foundation of knowledge information processing.

A distributed knowledge base control system, based on a large-scale relational database, is being developed, as are systems to support a distributed knowledge base utilization method aimed at parallel problem solving that will be run on the control system and to support higher-function knowledge acquisition.

Furthermore, a knowledge programming language and its processing system are being developed in order to trial manufacture a distributed knowledge base utilization experiment system.

4. Intelligent interface/software module

The study of a natural language includes context analysis, focusing on semantic analysis, which will provide a system by which sentences in junior-high-school science textbooks can be understood.

In addition, an interactive model structure that permits man-machine mutual understanding is being researched and developed, and intelligent interface verification software is being trial manufactured.

5. Intelligent programming/software module

This theme is intended for the pursuit of software engineering issues based on a logical programming language. The mid-term plan focuses on the design of a specification descriptive language, and proposes to amalgamate a

logic-based reasonable approach through a natural approach expressed in a natural language and graphics. The results of this research and development will be used in practical application fields to verify the results, and an intelligent programming verification software will be manufactured on an experimental basis.

6. Basic software verification system

This system is being researched and developed in order to apply the results of various R&D themes to practical application fields for the overall verification of these results and to feed back the results to each research theme.

Development Support System

A parallel software developing machine pilot model is being developed to support the trial manufacture of software for use in a language processing system in parallel-type kernel language version 1, initiated during the mid-term, and for a parallel inference mechanism based on the kernel language version 1.

This machine is a small-scale multiprocessor system in which multiple sequential inference-type machine CPUs are tightly coupled, and is used as a tool to implement parallel processing, on a process basis, as soon as possible and to identify the effectiveness of parallel processing.

Furthermore, more efficient software development for LAN systems is being attempted in order to expand and improve the software.

Supercomputers S-820/40, S-820/20 by Hitachi

43067613b Tokyo JECC NEWS in Japanese 1 Jul 88 p 3

[Article: "Highly Competitive Low-End Supercomputer by Hitachi With 30 Percent Share Projected--S-820 Group Within 8-to-1 Performance Range"]

[Text] Hitachi, Ltd., has developed and marketed two low-end models of the supercomputer "HITAC S-820 Group"--the S-820/40 with a peak ALU performance of 750 MFLOPS (the number of floating point operations executable per second, expressed in millions) and the S-820/20 with a peak ALU performance of 375 MFLOPS.

The S-820 Group currently is comprised of four models, ranging from the high-end model S-820/80, already on the market, to the low-end model S-820/20, and covers the wide 8-to-1 performance range.

The new models permit universities and national research institutes to employ their favorite UNIX when a single S-820 system is used with the existing vector processor control program "VOS3/HAP/ES."

The two models are scheduled to be shipped during the third quarter of this year, with the monthly rental starting at about ¥47 million for the S-820/40 and about ¥35 million for the S-820/20.

The monthly rental for the already-marketed high-end model S-820/80 starts at about ¥80 million, and that for the S-820/60 at about ¥57 million.

Supercomputers have been used to shorten R&D periods and reduce development costs, and more than 100 domestic installations are expected by the end of this year.

Hitachi has already reserved 24 models of the S-810 and S-820 and shipped 20 units, including 3 S-820s.

The new low-end models are expected to play important roles in expanding the market and developing new customers. Hitachi plans to receive orders for 70 S-820s (40 for the new models) in the next 5 years, with a market share of 30 percent.

The processors and related software of low-end models of S-820 feature:

1. Vector processing capability covering a wide 8-to-1 performance range

The 8-to-1 performance range is covered, from a peak ALU performance of 375 MFLOPS for the S-820/20 to 3 GFLOPS for the S-820/80, and lower level models may be field-upgraded to higher level ones.

2. Approximately twice the cost/performance of older models

The new models have processing capabilities about two times those of the older S-810 Group at about the same price.

3. Coexistence of UNIX

Under the control program VMS/ES involving a virtual computer system, the vector processor control program VOS3/HAP/ES can coexist with the UNIX System V based operating system HI-UX/M.

4. Improved supercomputer software development efficiency

FORT/AF is added to the conventional interactive development support system FORT/ASSISt to enhance FORTRAN program analysis support functions and simple document output functions of the analytical results.

DEQSOL E2, that automatically generates a supercomputer FORTRAN source program from a numerical formula, is enhanced and a large-scale simulation is implemented.

Hitachi has been promoting the expansion of circulating software under REFER (circulating software reference system), and has recently increased the menu to 27 pieces.

Studies Announced by Technical Research/Development Institute, Defense Agency

Gas Turbines for Vehicles, Cooling Efficiency

43062014 Tokyo BOEI GIJUTSU in Japanese Sep 88 pp 76-81

[Article by Yoichi Nakamura, technical official; Takaaki Shimazu, technical official; and Toru Yoshitomi, technical official, 2nd Motor Research Section, 2nd Division, 4th Laboratory: "Confirmation Tests on Performance of Main Components of Gas Turbine for Vehicle Use--Confirmation Test on Cooling Capacity of Cooling Cascade"]

[Text] 1. Purpose

Improved fuel consumption is indispensable to making a gas turbine practical for vehicle engines and it is necessary to ensure high temperature at the inlet of the turbine as well as to adopt a heat exchanger and a variable nozzle. To this end, the interiors of the turbine blades must be cooled. We have recently tested the cooling capacity of cooling turbine blades for high temperature use, using a cascade prototype produced in fiscal 1986. This is a report on the results of the test.

2. Method and Outline of Test

(1) Figure 1 gives a general illustration of the test equipment used. The tested blades and four dummy blades were fastened as a cascade in the wind tunnel and the performance test was conducted by forcing the flow of combustion gas through the tunnel and, at the same time, forcing the flow of cooling air through the interior of the tested blades.

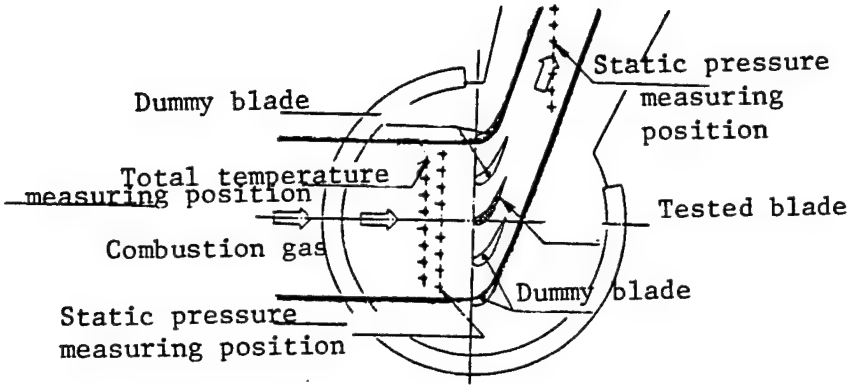

Figure 1. Outline of Experimental Apparatus

(2) Two-dimensional models about four times the scale of the real blade were used as tested blades and two types each for stationary and rotor blades were tested in various cooling structures. Figures 2 shows the internal cooling structure of the stationary blade. Also, temperature distribution was measured by embedding a thermocouple in the mean diameter on the blade surface.

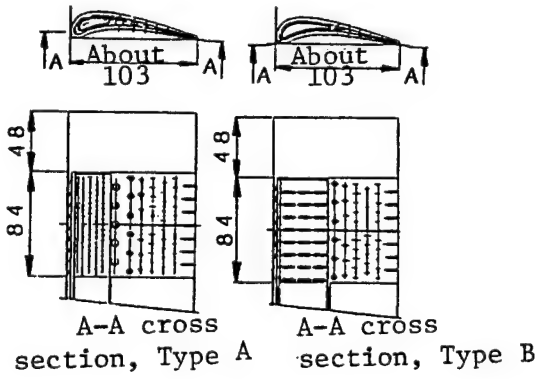

Figure 2. Internal Cooling Structure of Stationary Blade

(3) Test conditions were set so that total similarity to the real-blade conditions could be maintained by nondimensional parameters, such as Reynold's number, Mach number and biot number.

3. Results and Discussion

(1) In the stationary blade, cooling efficiency necessary to maintain the temperature of the blade member at less than 1,000°C is 42 percent or over. As the same time, occasionally the local maximum temperature for the combustion gas in the blade rotor reaches 1470°C.

Figure 3 shows test results with stationary blades, types A and B, at the design points. Both satisfy the required cooling efficiencies. Type B with a small variation is superior.

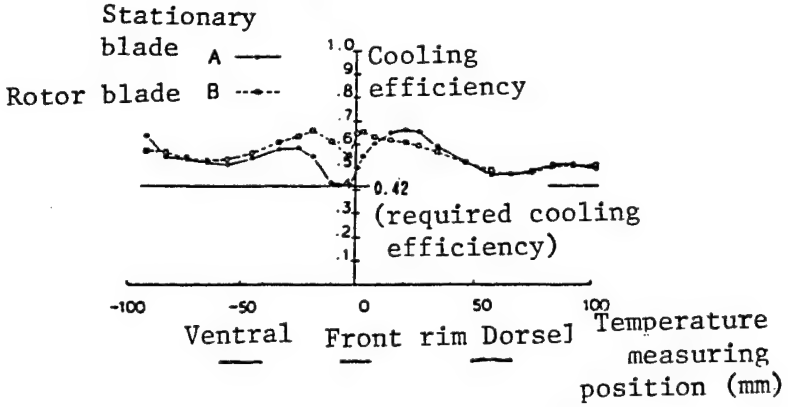

Figure 3. Test Results (Stationary Blade)

(2) In the rotor blade, cooling efficiency in the leading edge was lower than the requirement in both types A and B but, taking into consideration the effect of heat transfer acceleration by the surface roughness due to machining in the cooling passage in the process of real-blade manufacture, it seems to fully satisfy the requirement.

(3) In the rotor blade, average cooling efficiency on the mean diameter barely met the requirement but it greatly differed from the predicted value. We will study the reason for this from the results of future tests to visualize the flow in the interior of the blade.

Sensitivity of Explosives

43062014 Tokyo BOEI GIJUTSU in Japanese Sep 88 pp 76-81

[Article by Matsuo Kobayashi, 4th Ammunition Section, 1st Division, 1st Laboratory: "Semi-Empirical Analytic Study of the Sensitivity of Explosives (Part 1)"]

[Text] 1. Purpose

In recent years, with the speedup of computation by large computers and their increased memory capacities, various programs making it possible to predict the reactivity and stability of chemical substances without experiment have been reported. This method can accurately predict handling simple substances but involves some difficulties in handling mixed explosives used for equipment or explosives containing polymeric resins. Predicting the sensitivities of these explosives is absolutely necessary to develop high explosives and it is hoped that simple and practical prediction methods will be devised.

It has been pointed out that there are limits to predicting the reactivity and stability of chemical substances from their composition and structure but many researchers since Van't Hoff have insisted that molecular structure characteristics, such as the contents of oxygen and nitrogen in molecules and the concentrations at which functional groups exist, have something to do with the reactivity and stability of these molecules.

In this Report No 1, we analyzed the drop hammer sensitivity of explosives on the basis of their molecular structure characteristics and using test results studied the propriety of the analytic method used and the possibility of predicting their sensitivity.

2. Method and Details of Test

(Parameters used for analysis)

The parameters used for analysis were oxygen balance, nitrogen content and 14 structural formulas. The structural formulas used are shown in Table 1.

Table 1. Structural Formulas

$-C-O-NO_2$		$-C-NO_2$
$-C-N-NO_2$		$-N \cdot HNO_3$
$-N \cdot HClO_4$		$-N-N$
$-N=N-$	$>C=N-$	$>C-N-$
$AR-O-$	$AR-C=O$	$AR-NO_2$
$AR-NH_2$	$AR-Cl$	AR is benzene ring

(Model function)

- Explanation of symbols -

[IS] : Drop hammer sensitivity
[NP] : Nitrogen content
[OB] : Absolute value of oxygen balance
[MS] : k(K = 1 ~ 14): Structural parameter
[IS] = F ([OB], [NP], [MS] k)

We prepared various model functions F presented above using the test results and making the closest square-law approximation. Then we obtained the coefficients of the model functions and coefficient errors.

Test Results

We acquired experiment report values of about 60 types of single explosives from documents.

[Application to mixed explosives and explosives containing polymeric resins]

Table 2. Experimental Values and Computed Values of Drop Hammer Sensitivity (unit: Nm)

Name of explosive	Experimental value	Computed value	Computed value (II)
Ammonium nitrate	50 or more	48	48
Ammonium perchlorate	15	15	12
Dinitrotoluene	50 or more	50	55
Trinitrobenzoic acid	10	9	7
Tetramethylenetetranitramine	7.4	6.3	7.3
Trinitrophenol	7.4	7.3	7.8
Trinitrophenzene	7.4	8.7	8.5
Trinitrotoluene	15	15	17
Trimethylenetrinitramine	7.4	9.0	5.7
Trinitrophenylmethylnitramine	3	3	5
Trinitroaniline	15	13	16
Tetranitropentaerythritol	3	3	2
Ethylenedinitramine	8	8	7
Nitroglycerin	0.2	0.2	0.7
Nitroglycol	0.2	0.2	0.6

We computed Comp. B, Octol and three types of PBX, using the coefficient of each of the above single explosives, and compared the results with the test results.

3. Results and Discussion

We learned that drop hammer sensitivity and molecular structure characteristics for the 60 types of single explosives used for our analysis could be approximated by the following functional relations.

$$\log[IS] = a_1[NP] + a_2[OB] + \sum_{K=1}^{14} b_K [MS]_K$$

For those 15 of the 60 types of explosives where the values of both precipitating energy and explosion heat were known, we included these values as parameters and analyzed their sensitivity separately. Table 2 shows the results of computed values (I) including activation energy and explosion heat and computed valued (II) not including them with respect to these 15 types of explosives.

Comp. B and Octol agreed well with the test results by using the coefficient of each of the component single explosives and the weight mixing ratio.

Similar results were obtained for the PBX-group explosives

Optical Fiber Echo Sound Receiver

43062014 Tokyo BOEI GIJUTSU in Japanese Sep 88 pp 76-81

[Article by Takayoshi Hyodo, technical official and Hiroyuki Mikami, technical official, 1st Acoustic Section, 1st Division. 5th Laboratory: "Test on Optical Fiber Echo Sound Receiver of Interference Type"]

[Text] 1. Purpose

Output fluctuation due to temperature is so great with underwater echo sound receivers that it is a factor preventing them from becoming practical. This is a report on the basic experiment we conducted to stabilize the output of the most common optical fiber echo sound receiver of the Mach-Zehnder interference type.

2. Method and Details of Test

Figure 1 shows the composition of the echo sound receiver we tested. It extracts as light intensity the phase change of light of the optical fiber due to sound pressure by causing it to interfere with light of the

optical fiber due to sound pressure by causing it to interfere with light of the reference fiber. Phase change also occurs to the fiber by slight temperature change and appears as signal output fluctuation. This fluctuation must be suppressed to enable the device to be used as an echo sound receiver. Here, we used the formulas to drive the cylindrical piezoelectric vibrator coiled with the reference fiber by the output fluctuation component (DC component) and cause the expansion/contraction of the reference fiber so as to offset phase change by the temperature of the receive fiber. We used the light modulation formula to stabilize the detection of receive signals. Semiconductor laser (wavelength: 1.3 μm) was used for light. a [polarized surface preserving fiber (length: about 22 m) was used for optical fiber and a photo coupler was used for the bifurcation of light. The test was conducted using a 5th Laboratory water tank.

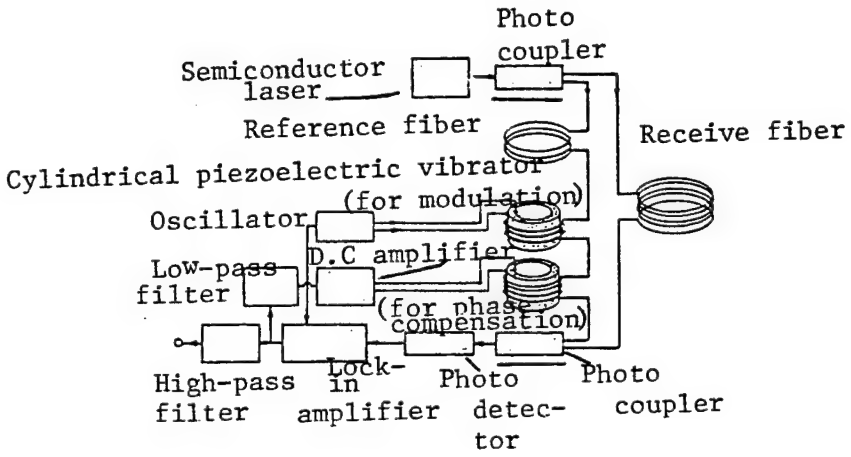

Figure 1. Composition of Optical Fiber Echo Sound Receiver Tested

3. Results and Discussion

(1) Results

a. Figures 2 shows the results of FFT analysis of output at the time of incidence of continuous waves with sound pressure of about 100 dB (0 dB = 1 μPa) and frequency of 3 kHz. The SN ratio was about 50 dB.

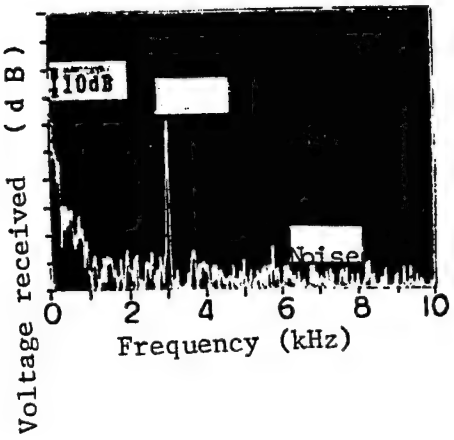

Figure 2. Example of Frequency Analysis of Receive Output

b. Figure 3 shows the input signal in the case of transmission of a pulse modulated wave. The receive waveform was satisfactory.

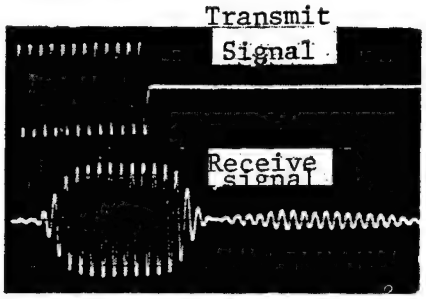

Figure 3. Input Signal of Pulse Modulated Wave (frequency: 3 kHz; pulse width: 4 ms)

c. Figure 4 shows the output fluctuation suppressing effect.

(a) Is the case without suppression and (b) is the case with suppression? The periodic fluctuation of the time when temperature continuously changes is suppressed but temporal drift is not completely eliminated.

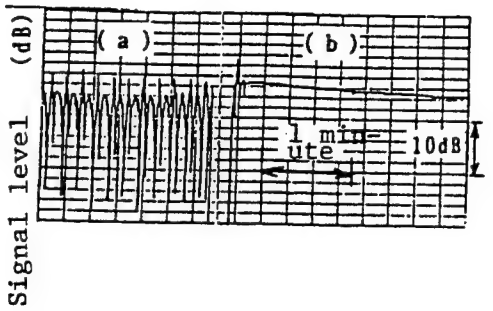

Figure 4: Output Fluctuation Suppressing Effect (a) Case without suppression (b) Case with suppression

(2) Discussion

a. We confirmed the output fluctuation suppressing effect with a piezoelectric vibrator. Some of the temporal drift remained but this presumably was because the adjustment of compensation for large phase changes was insufficient.

b. An optical fiber echo sound receiver of the interference type has high wave receiving sensitivity. (The wave receiving sensitivity was about -160 dB (0 dB = 1 V/μPa). But its output stabilizing circuit is complicated. For practical use, it is necessary to further study means of output stabilization including optical fiber echo sound receivers of other formulas.

Simulating Underwater Reverberation

43062014 Tokyo BOEI GIJUTSU in Japanese Sep 88 pp 76-81

[Article by Yasushi Sudo, technical official, 1st Underwater Weapons Research Section, 2nd Division, 5th Laboratory: "On Improvement of Method to Simulate Underwater Reverberation"]

[Text] 1. Purpose

The technology of simulating reverberation in the underwater sound field is closely related to improved target detecting technology and the testing and evaluating technology. The purpose of this report is to improve simulation so that it may be easier and faster than by methods known to date (REVGEN and REVSIM).

2. Method and Details of Test

This report is based on the F.O.M. theory. We obtained a formula of reverberation suitable for simulation by extracting stochastic parts only from the reverberation formula based on this theory and expressing their statistical properties by means of complex normal white noise.

3. Results and Discussion

(1) Results

We extracted stochastic parts and, to analyze their statistical properties, generalized the Doppler density matrix (DDM) used in REVGEN. This generalized DDM is defined by continuous time and expressed using a solid angle. The formula or reverberation led by these and its block diagram are shown below.

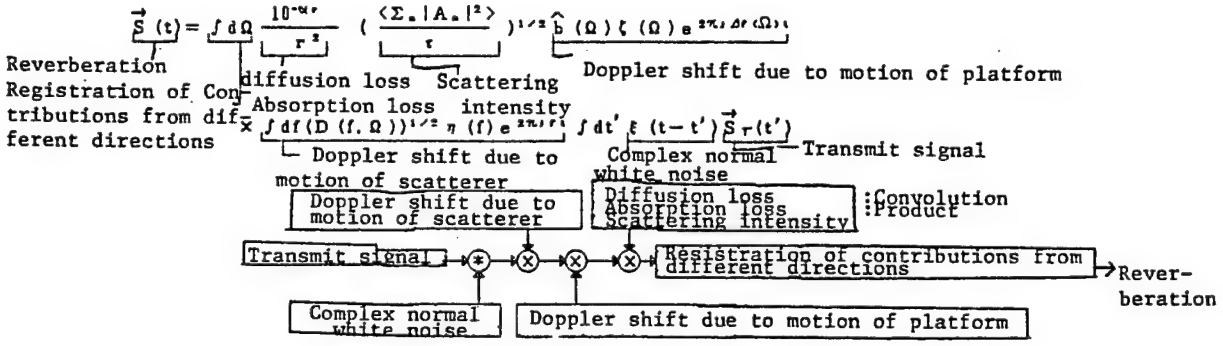

(S(t): matrix vector composed of veverberation at each receive beam, Ω: solid angle, Sr(t): matrix vector composed of transmit waveform of each transmit beam (0 for t < 0), ξ(t), η(f), ζ(Ω): complex normal white noise, D(f,Ω): stochastic density of Doppler shift of scatterer, $\langle \sum n |A_n|^2 \rangle$: quantity proportionate to mean scattering intensity of scatterer, $\Delta f(\Omega)$: Doppler shift due to motion of platform, τ: duration of transmit signal, b(Ω): matrix composed of beam pattern at time of transmission/reception)

This formula also showed that the reverberation vector could also be expressed in the form of the sum of contributions from reverberation of sea surface, volume and sea bottom.

(Discussion)

This method takes reverberation as a stochastic process; therefore, it can simplify the procedure required by the scatterer simulation of REVGEN. It can also directly express the randomness of angles and thus enables correlation between beams to be considered without solving the matrix equation of REVSIM.

Metallic Fuel Burner

43062014 Tokyo BOEI GIJUTSU in Japanese Sep 88 pp 76-81

[Article by Somigo Ko, technical official, and Ikuo Koida, technical official, 4th Underwater Weapons Research Section, 2nd Division, 5th Laboratory: "On Simulation Model of Metallic Fuel Burner"]

[Text] 1. Purpose

The reaction of metallic lithium (Li) and sulfur hexafluoride (SF_6) is known as a heat source for power plants with large caloric power and not generating exhaust gas. We prepared a simulation model concerning the thermal output of a burner to generate high-pressure steam, taking advantage of this heat of reaction of metallic lithium and sulfur hexafluoride, with the object of deciding combustive conditions for combustion tests and predicting its thermal output. When we compared the fluctuation of thermal output of the burner obtained by computation from this simulation model with experimental data, we learned that the model could simulate the operation of the burner well. Hence, this announcement of the result.

2. Method

Figure 1 shows the burner that we simulated. Heat generated through the reaction of Li and SF_6 is partially consumed to maintain the temperature of the lithium but the rest moves to the water pipe wall by the flow caused by the jetting of SF_6, transmitted to the water and the steam by heat transfer on the surface of the wall and heat conduction through the interior of the wall and generates super-heated steam. In computing this heat movement, we obtained the coefficients of heat transfer of lithium and the water pipe wall from experimental data because they are affected by the SF_6 jet amount and difficult to compute by theory. The basic equations for the simulation model are as follows:

$$C_L M_L \frac{dT_L}{dt} = Q_{SF} - Q_M$$

from the heat balance in the interior of the burner.

$$A_W \gamma_W \frac{\partial h_W}{\partial t} = -G \frac{\partial h_W}{\partial x} + q_W$$

from the heat balance in the interior of the water wall.

Symbols: T_L, C_L, M_L, Q_{SF} and Q_M: temperature, specific heat, weight, calorific power and amount of heat transfer of lithium

h_w, γw, G, q_w and A_w: enthalpv, specific weight, weight flow and amount of heat transfer of steam and cross-sectional area of water pipe

t and x: time and distance from inlet of water pipe

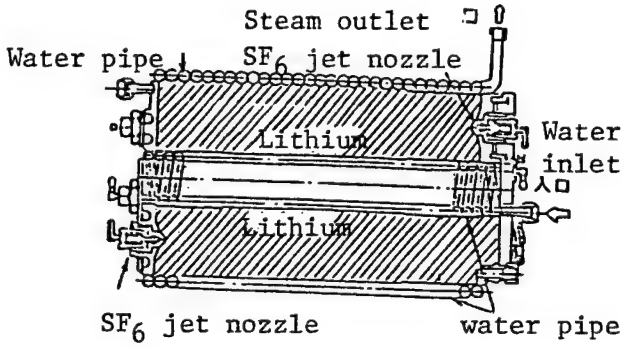

Figure 1. Burner

3. Results and Discussion

Figure 2 compares the results of simulation of the temperature pressure of steam of the time when SF_6 jet amount and water supply were changed and the experimental results. From this, we consider that this simulation model agrees with the experimental results except for part of the steam temperature test and can simulate the burner well and thus, can contribute to the development of future studies.

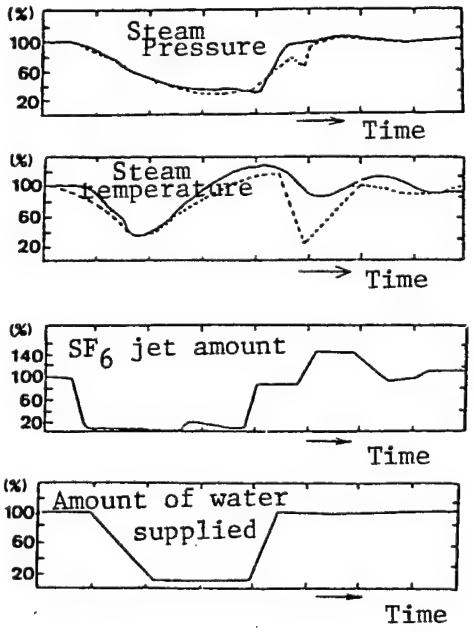

Figure 2. Comparison of Simulation and Experimental Data

Advances in Ceramic Sensor Technology

Monolithic Ultrasonic Sensor

43067500 Tokyo NEW CERAMICS in Japanese Jul 88 pp 37-40

[Article by M. Okayama, assistant professor of electrical engineering, Fundamental Engineering Department, Osaka University, and Y. Hamakawa, professor of electrical engineering, Osaka University]

[Text] 1. Preface

Human ears are capable not only of sensing sounds but can also identify the sources of sound based on the associated tones, pitches and directions. The mechanical version of the human ear is the ultrasonic sensor. When this sensor detects a sound wave from an object, it irradiates the object with ultrasonic waves and receives the reflected waves, thereby sensing the distance, configuration and mechanical properties of the object. This is accomplished without contact with the object and at a high speed. The sensor is used in practice for such things as level gauges, flow meters, viscosimeters, fish detectors, flaw detectors and ultrasonic diagnosis equipment.[1]

Because the ultrasonic sensors used in such pieces of equipment are primarily elements in which horns and sound absorbing materials are mechanically fitted into piezoelectric ceramics,[2] they can not be integrated with the signal amplification sections and this creates a problem in terms of their size. This, in turn, creates a problem with regard to their practical application.

The development of a so-called intelligent sensor in which the sensor and signal processing sections are integrated would serve to solve this problem and could be more widely applied. Other approaches to enhancing the effectiveness of ultrasonic sensors include developing phased arrays, increasing sensitivity and simplifying connections with microcomputers.

From this perspective, the authors have proposed and created a monolithic silicon sensor in which the ultrasonic detecting section is provided on the silicon substrate. In other words, thin films made of PLZT, PLT and $PbTiO_3$--which have favorably strong diaelectricity, piezoelectricity and pyroelectricity--have been produced, and a monolithic silicon sensor using these materials has been developed.[3] A thin film of $PbTiO_3$, whose piezoelectricity is excellent, was grown on a microcantilever on a silicon substrate produced using microprocessing technology in order to create an ultrasonic sensor. This article summarizes the principle, production method and fundamental characteristics of this ultrasonic sensor.[4, 5]

2. Element Construction and Operation Analysis

Figure 1 shows an example of the element construction of a $PbTiO_3$ thin-film ultrasonic sensor. The platinum, $PbTiO_3$ and aluminum films are produced on the Si or SiO_2 microcantilever, scored to hundreds of μm in length and scores of μm in width. Mechanical coordination between this construction and the air is good. If an ultrasonic wave strikes this sensor, the cantilever vibrates and the piezoelectric effect due to the stress of a $PbTiO_3$ film generates a current that is detected as an ultrasonic wave. This construction allows a number of cantilevers to be arrayed on the Si substrate. Consequently, one-dimensional and two-dimensional array sensors can be realized. Also, a spectrum analyzer can be created by changing the length of the cantilever.

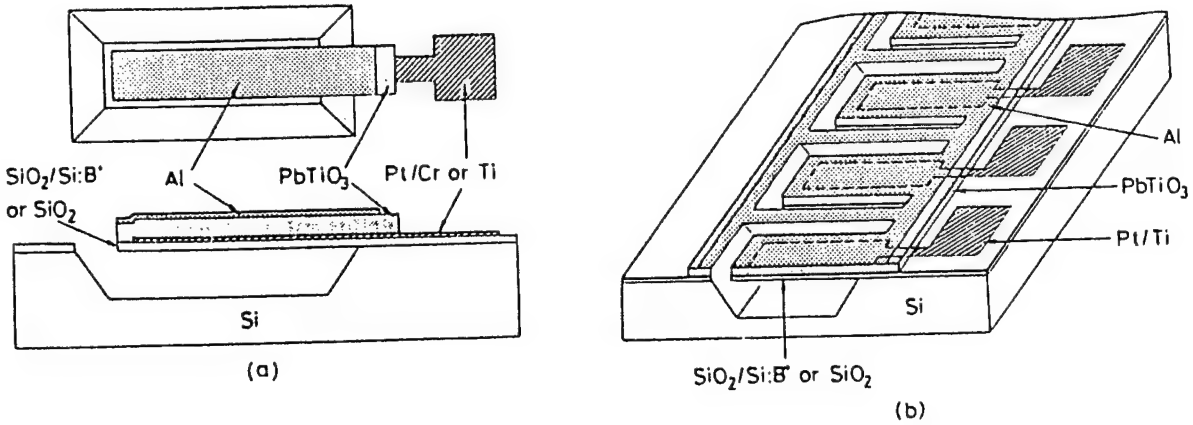

Figure 1. Construction of $PbTiO_3$ Thin Film Ultrasonic Sensor

As indicated in Figure 2, a cantilever can be bent with a uniform force (F). In this configuration, an electric charge is generated in the $PbTiO_3$ due to piezoelectricity, and a voltage (V) described by the following formula is generated between the electrodes.

$$V = \frac{d_{31} t_2 F(\ell + \ell_a)(h_a - h_b)}{2I\varepsilon_o\varepsilon_r} \qquad (1)$$

In this formula,

d_{31}= piezoelectric constant of $PbTiO_3$
t_2= thickness of $PbTiO_3$
$\varepsilon_o\varepsilon_r$=diaelectric constant of $PbTiO_3$
I=secondary moment of equivalent cross-section in terms of $PbTiO_3$
h_α, h_b=thickness of upper and lower parts of $PbTiO_3$ from the neutral surface on which no stress is placed

The length of the upper electrode is equal to the length of the bottom of the cantilever (ℓ), or $\ell - \ell_a$.

According to formula (1), the following requirements are favorable for increasing V.

a. d_{31} is large and ε_o-ε_r is small from the standpoint of physical property.

b. From a construction standpoint, ℓ_α is large--the electrode is located in proximity to the bottom of a cantilever--h_α is larger than h_b, and t_2 is large.

A cantilever will resonate at several frequencies. This resonant frequency, f_R, is determined from the kinetic formula of vibration.[6]

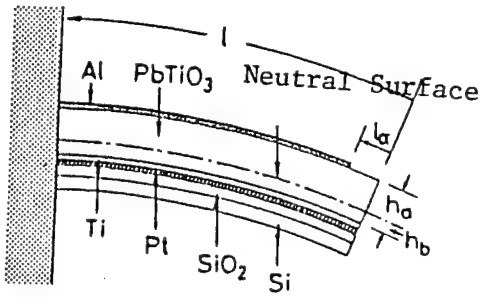

Figure 2. Cross-Sectional View of Cantilever Bent by a Uniform Force

$$f_n = \frac{3.52\Lambda_i}{2\pi}\sqrt{\frac{E_2 I}{\mu \ell^4}} \qquad (2)$$

In this formula,

μ=weight of a cantilever per its unit length
E_2=Young's modulus of $PbTiO_3$
Ai=constant of ith vibration.

According to formula (2), fR is reciprocally proportional to the second power of the length of a cantilever.

3. Production of Ultrasonic Sensor

3.1 Production of Microcantilever by Anisotropic Etching

A procedure like that depicted in Figure 3 is performed to produce a Si microcantilever on the Si substrate. SiO_2 with the pattern shown in 3(a) is initially produced on a [100] Si substrate in which high-density boron (B) is dispersed to form an oxide film. This is done using photolithography technology. The straight line direction of the pattern is [110]. The pattern of the SiO is opposite to the above pattern, and the boron (B) is not dispersed. Instead, the silicon is etched using a mixed liquid (EPW) consisting of ethylene diamine, pyrocatechol and water. The etching speed of the Si [111] surface using EPW is small, while that of the other Si [100] and [110] surfaces is large.[7] Also, the etching speed of Si and SiO_2 surfaces doped with boron at a high density is low. If the Si substrate as depicted in Figure 3 (a) is etched, a V-shaped groove as shown in 3(b) is produced, and the Si is further removed from the corners of the cantilever section as shown in 3(c). After satisfactory etching, the Si cantilever shown in 3(d) is produced.

3.2 Growth of $PbTiO_3$ Thin Film

To grow thin films of multioxides such as PLXT and $PbTiO_3$, a high-frequency sputtering process was used because the crystallographic and electric properties of the thin films were good and the associated equipment was easily procurable. Because the sputtering gas can be easily reduced during the growth of $PbTiO_3$, argon mixed with 10 percent oxygen was used. The Pb_3O_4 was mixed with TiO_2 and calcined. The $PbTiO_3$ powder thus produced was placed on a quartz plate as a target. Since steam pressure for Pb is higher than that for Ti, and since Pb tends to be insufficient in the thin film, the amount of Pb_3O_4 added is 10 percent by weight more than that of its stoichiometrical composition. The growth speed is 30-40 Å. The films accumulated on the Pt and Si

substrates are multicrystals with a square crystal-based perovskite shape, as a result of X-ray diffraction and SEM observation. They consist of a number of grains. These films follow a pattern of epitaxial growth on the single-crystal substrate of oxides such as MgO and $SrTiO_3$[9] and orient to the C axis on the fluoride film and the spinel film on Si.[10,11] Also, the quality of the films is improved by applying microwaves to the plasma in the sputtering process.[10]

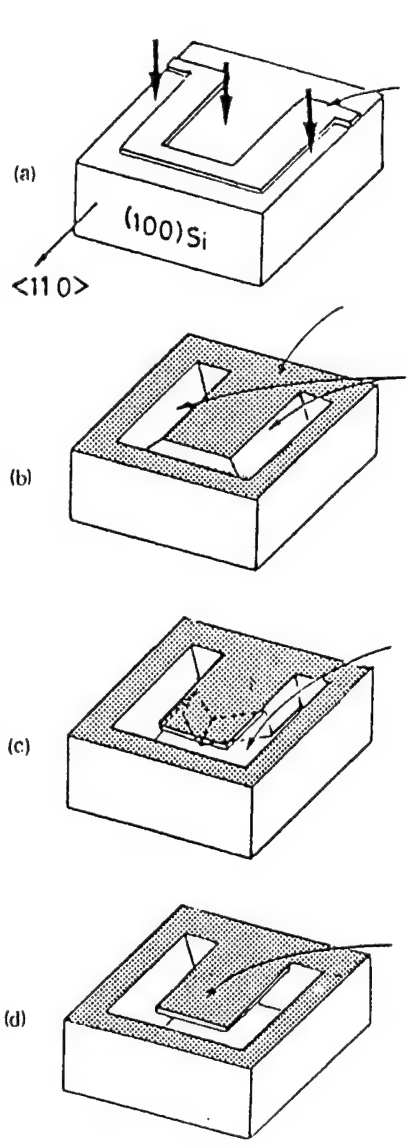

Figure 3. Production Process of Si Cantilever

The $PbTiO_3$ film on the Pt substrate is noncrystalline at a substrate temperature of 350°C or less. At a temperature of 350°C or more, the film achieves crystal growth, and the crystal construction changes from the pyrochroite shape to that of perovskite with the rise in the temperature of the substrate. Furthermore, the dielectric constant ε and the residual polarization Pr increases. However, if the temperature is too high, the $PbTiO_3$ dissolves and ε and Pr become small. Also, ε and Pr increase with the thickness of a film, and ε and Pr become saturated at - 1 μm or more and at - 2 μm or more, respectively. In light of this dependence, a thin film having a substrate temperature of 500-500°C, and $\geq$ approximately 2 μm in diameter is suitable.

4. Characteristic of Response to Ultrasonic Wave

With regard to the ultrasonic response of these trially fabricated elements, the ultrasonic wave generated from the PZT piezoelectric transducer was irradiated on a sensor placed opposite, and the output of the sensor was amplified with a lock-in amplifier and detected.

Figure 4 shows the dependence of sensor sensitivity on the frequency in proximity to the resonance point. This sensor is provided with a Si cantilever 250 μm in width and 650 μm in length. This figure tells us that sensitivity peaks at the basis resonance frequency of 6.5 KHz, a higher-order mode of 35 KHz, and also at 95 KHz, due to the bending vibration in the longitudinal direction. The maximum sensitivity in the vicinity of 35KHz becomes -102dB (1V/μbar is estimated at 0dB). This sensitivity is very small compared with the sensitivity of -60dB of ceramic elements sold on the market. However, a sensitivity of -80dB can be obtained from an element provided with an electrode only in close proximity to the fixed end, as shown in Section 2, on a Si cantilever 0.5 mm in width and 1.5 mm in length. The value d_{31} of the $PbTiO_3$ film obtained from the sensitivity is 4.3×10^{-12} C/N, being almost equivalent to the value of a ceramic.

Figure 5 shows the dependence of the secondary resonant frequency on the length of the cantilever. The measured values coincide well with the theory of formula (2), which says they will be reciprocally proportional to the second power of the length of the cantilever (solid line in the Figure). Thus, the resonant frequency can be easily changed by changing the length of the cantilever. When a Si cantilever is used, the resonant frequency of the second mode changes from 10 KHz to 1 MHz, if the length of the cantilever is changed from 100 μm to 1000 μm. The output voltage is proportional at the double-digit sound pressure. If this voltage is proportional up to the stress point at which the cantilever is destroyed, the dynamic range becomes - 5 digits.

The mark (O) in Figure 6 shows the directivity of the single element with a cantilever length of 500 μm, at 151KHz. The solid line is a theoretical curve for the isotropic characteristic, and the measured values coincide well with this curve. Also, the mark (●) shows the directivity of three elements placed in a row at an interval of 1mm, and this directivity has increased.

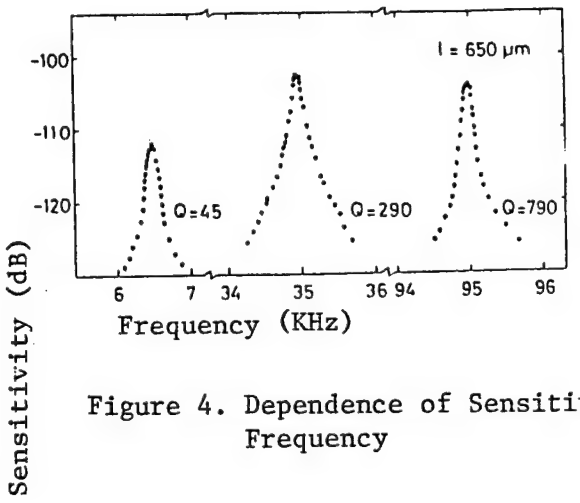

Figure 4. Dependence of Sensitivity of Sensor on Frequency

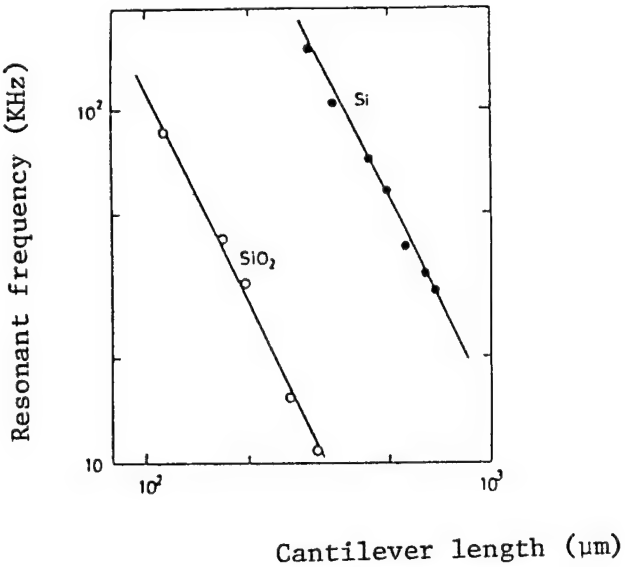

Figure 5. Dependence of Resonant Frequency on Cantilever Length

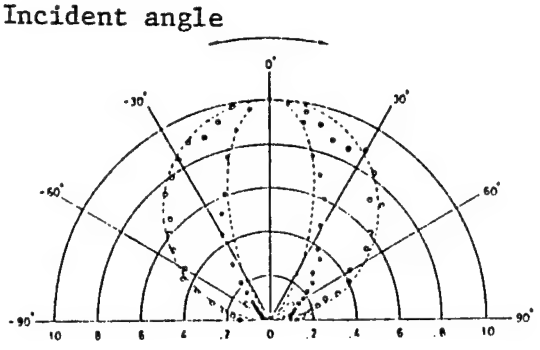

Figure 6. Directivity of Ultrasonic Sensor
O: 1 element, ●: 3 element array,
dashed line: theoretical curve

5. Array Sensor and its Features

The cantilevers are placed in a row and are placed so that they are arrayed according to the signals to be processed. As a result, these cantilevers are capable of performing more advanced functions such as polarization and translation. In other words, the electric delay in and the combination of each output from the sensor array allow directivity for the entire sensor. The block diagram in Figure 7 shows the directivity of the measuring system. Some output of the linear array is synchronized so that the directivity is increased. Furthermore, this output is electrically translated, and the output of the plane array is delayed and polarized, thereby scanning the detection direction.

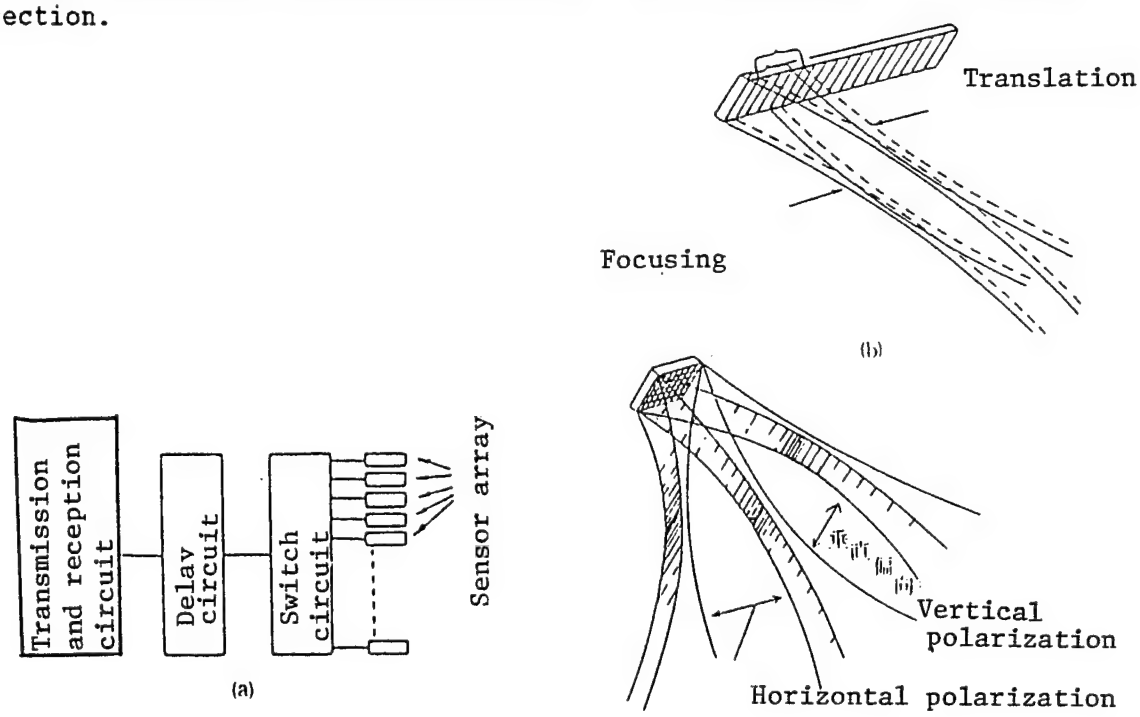

Figure 7. Change in Directivity According to Sensor Array

6. Conclusion

The monolithic silicon ultrasonic sensor using a thin film of $PbTiO_3$ has been described above. Because this sensor features a monolithic silicon construction, it can be used for an intelligent sensor to be integrated with an IC that includes a signal processing circuit. Consequently, it is expected that this sensor will foster the development of more advanced and inexpensive ultrasonic sensing technology.

References

1. "Elecera" Publishing Committee, eds. Ceramic Sensor: Technical Literature (1979).

2. M. Okuyama and Y. Hamakawa. System and Control, 30 No. 11 694 (1986).

3. M. Okuyama and Y. Hamakawa. Ferroelectrics 63 242 (1985).

4. M. Kojima, M. Sunagawa, H. Seto, Y. Matsui, M. Okuyama and Y. Hamakawa. Proc. 2nd Sensor Symposium (1982).

5. K. Ohtani, M. Okuyama, and Y. Hamakawa. Jpn.J.Appl.Phys. 23-1 133 (1984).

6. J. P. Hartog. Mechanical Vibration (McGraw-Hill, New York, 1956).

7. R. M. Finne and D. L. Kleine. J. Electrochem. Soc. 114 965 (1967).

8. M. Okuyama, Y. Matsui, H. Nakano and Y. Hamakawa. Ferroelectrics 33 235 (1981).

9. M. Okuyama, T. Usuki, Y. Hamakawa and T. Nakagawa. Appl.Phys. 21 339 (1980).

10. M. Okuyama, T. Ueda and Y. Hamakawa. Jpn.J.Appl.Phys. 24 619 (1985).

11. S. Matsubara, N. Shohata and M. Mikami. Jpn.J.Appl.Phys. 24-31 10 (1985).

Superconducting Sensor

43067500 Tokyo NEW CERAMICS in Japanese Jul 88 pp 49-52

[Article by S. Tsuchimoto, manager of Research Department No. 3 of the Central Institute of Research, Sharp Corporation Technology Division, and also by H. Nojima, Assistant Manager of Research Department No. 3]

[Text] 1. Preface

Since the discovery of ceramic high-temperature superconductors, which greatly exceed the critical temperature (Tc) of conventional metal-based superconductors,[1,2] investigators from the industrial, governmental and

academic sectors have been actively engaged in fundamental and applied research. Their goal is to improve the critical temperature and critical current density, and also to create new electronic elements.

If superconductors with a critical temperature close to normal room temperature can be created, and if the corresponding application devices and systems are configured, great innovations can be made in the fields of electronics, means of conveyance, and energy. Thus the potential impact on human society is very great.

We have focused our attention on the critical phenomenon--how a superconductor is transformed into superconducting conditions--and have conducted research on applying high-temperature ceramic superconductors to electronic elements, especially sensors. Against this background, we have examined in depth the electric behavior of a ceramic superconductor in the presence of a magnetic field. We learned that the behavior of the superconductor is quite different from the magnetic reluctance effect displayed by conventional semiconductors and magnetic substances. last summer, we reported the possibility of creating an unprecedently high-performance magnetic sensor using this effect. This sensor has the following excellent features:

1. It is possible to carry out a highly sensitive measurement of the magnetic field using the sudden change in the resistance in the low magnetic field region.

2. The sensor can be used for digital as well as for analog measurement.

3. The production of an element does not require advanced technology such as that needed to produce a Josephson device.

4. Handling the element is very simple.

A superconducting film of Y-Ba-Cu-O was produced using the spray pyrolysis method and the element was configured in a zigzag shape. This made it possible to create a highly sensitive magnetic sensor (superconducting resistance M-type sensor). Our report on this sensor is as follows:

2. Sample Preparation and Material Characteristics

The superconducting Y-Bu-Cu-0 film was produced by the spray pyrolysis method. A superconducting thick film is easily produced by this method, which does not require vacuum equipment.

3. A water solution of $Y(NO3)_3$, $6H2O$, $Ba(No_3)_2$, $Cu(NO_3)_2$, $3H_2O$ was adjusted to the specified concentration, and a spray solution was made. Yttrium stabilized zirconia (YSZ) was used as a substrate, and the spray solution was sprayed on the substrate at a constant temperature of $350^{o}C$.

A film adhered after the sprayed solution was heat-treated at 800°C in air for 5 minutes. Subsequently, a second film layer was added by repeating the spraying process under the same conditions. This produced a thick film of about 5 μm. After production of the spray film was completed, a final heat treatment was carried out at 950°C for 5 minutes and a sample was produced.

This sample was analyzed by X-ray diffraction and EPMA. The sample showed a crystal structure of $Y_1\ Ba_2\ Cu_3\ O_{7-x}$ with its C axis oriented vertically to the surface of the substrate. Also, an observation of the sample using a scanning electron microscope (SEM), showed that the sample was composed of a number of particles (granular diameter, 2-5 μm.

Ti electrodes were formed on this sample through vacuum evaporation, and the electric characteristics of the sample were measured. Figure 1 shows the dependence of electric resistance on temperature. These data were obtained by the normal four-terminal method. In this case, a sample 5 mm in width was used and the distance between the voltage electrodes was set at 5 mm. figure 1 tells us that the electric resistance begins to greatly decline at approximately 100K, and becomes 0 at 80K. Also, it was confirmed, as a result of measuring magnetic susceptibility, that the above sample showed a superconducting transformation at almost the same temperature.

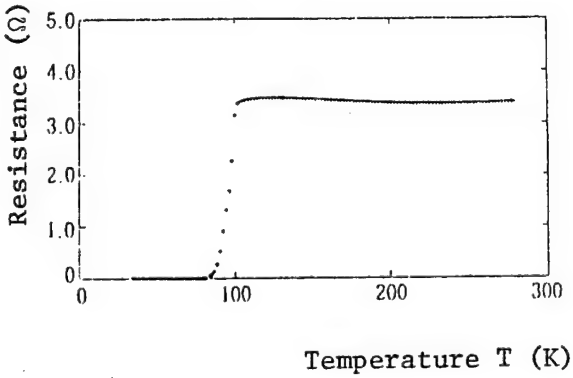

Figure 1. Dependence of Electric Resistance of Y-Ba-Cu-0 Thick Film Sample Produced by Spray Pyrolysis Method on Temperature

3. Characteristics of Element

Figure 2 shows the dependence of electric resistance on the magnetic field strength of the sample. This is done by using the value of the electric current, which flows into the sample at 77K, as a parameter. When the magnetic field is applied, the sample suddenly displays electric resistance, whereas its electric resistance previously was 0.

This resistance continues to increase as the strength of the magnetic field increases. This characteristic depends on the value of the electric current flowing into the sample. The greater this value, the greater the electric resistance that appears with the magnetic field and the steeper the increase in this resistance. The strength of the magnetic field with which the resistance suddenly appears shifts to the low magnetic field side with an increase in the electric current.

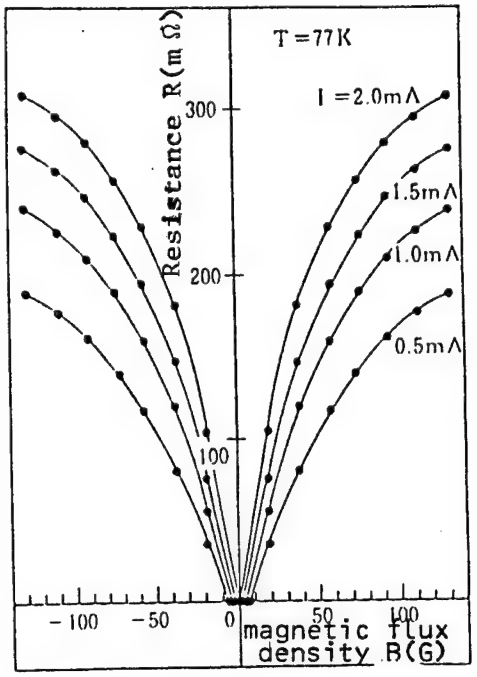

Figure 2. Magnetic Resistance Characteristic of Y-Ba-Cu-O Thick Film Sample at 77K

The above results are consistent with the behavior of the bulk element,[4, 5] which has already been reported. However, the sample produced by the spray pyrolysis method shows a magnetic resistance greater than that of the bulk element. The sample with this characteristic was processed in a zigzag shape, as shown in Figure 3, in order to produce an element. We named this element a superconducting magnetic resistance M-type sensor (hereinafter referred to as 'M-type sensor'). By processing the element in a zigzag shape, the width of the electric current route can be narrowed. At the same time, magnetic resistance can be increased by increasing the length of the electric current route. The width and length of the electric current route of this particular element were 0.7 mm and 72 mm, respectively.

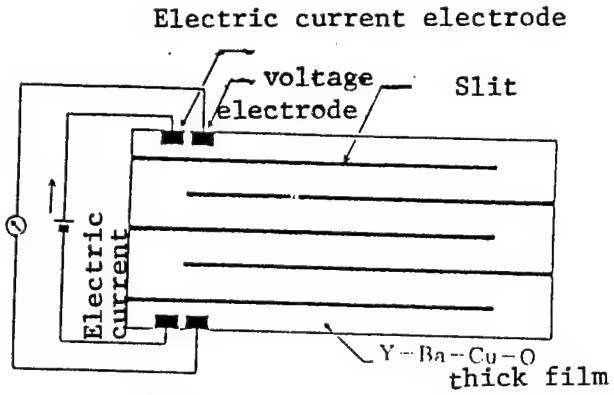

Figure 3. Basic Construction of Superconducting Magnetic Resistance M-Type Sensor

Figure 4 shows the dependence of the electric resistance of the M-type sensor on the strength of the magnetic field when the value of electric current flowing into the element, which is used as a parameter, was set at 77K. This element shows the same behavior as the magnetic resistance characteristic of the sample that was not processed in a zigzag shape, as shown in Figure 2. However, it is understood that the zigzag processing of the element has served to increase magnetic resistance.

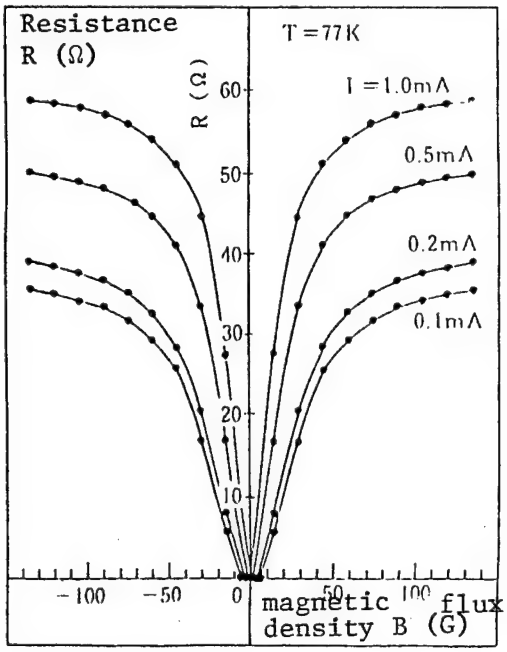

Figure 4. Magnetic Resistance Characteristic of Superconducting Magnetic Resistance M-Type Sensor

The sensitivity of the magnetic resistance element is defined by the maximum increase rate $(\Delta R/\Delta B)_{max}$. Each sensitivity for the bulk element reported previously, for the thick-film, element that was not processed in a zigzag shape and for the M-type sensor is shown in Figure 5 as a function of the electric current flowing into the element. This Figure shows that the sensitivity of the M-type sensor has rapidly increased.

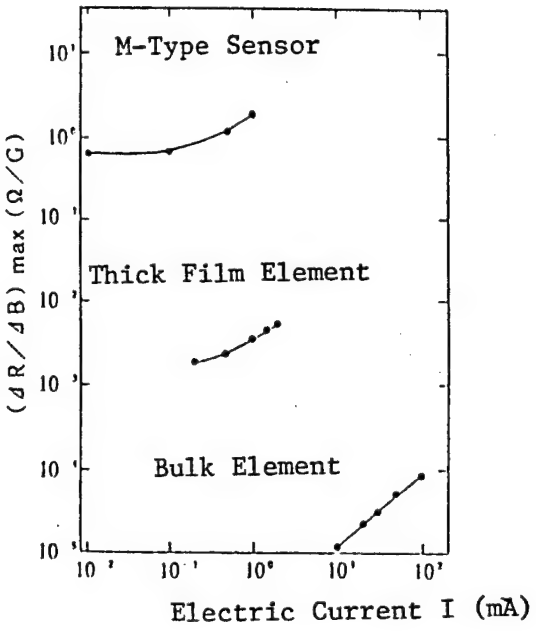

Figure 5. Comparison of Sensitivity of Bulk Element, Thick Film Element Not Processed in Zigzag Shapes, and M-Type Sensor

4. Observation Regarding Operating Mechanism and Increase in Sensitivity

The operating mechanism associated with the magnetic resistance characteristic of a ceramic superconductor is as follows:

The ceramic superconductor is a multicrystal consisting of a number of superconductor particles. At the boundary between these particles, very thin insulating materials must be present or the contact portion between the particles becomes point-shaped. In other words, the ceramic superconductor can be regarded as a so-called superconducting assembly that is weakly bonded. In the case where the magnetic field is very weak, a superconducting current can flow into this weak bond portion with a resistance of 0, due to the Josephson effect. If a magnetic

field is applied, however, the critical Josephson electric current decreases, and it is thus difficult for the superconducting current to flow into the weak bond portion. As a result, it is thought that electric resistance suddenly appears.

Next, we will look at the increase in sensitivity. It was first thought that the great increase in the sensitivity of the M-type sensor was caused by the effect of the configuration. The narrow width of the electric current route and also the increased length of this route allow electric resistance to be increased under the advent conditions of this resistance during application of the magnetic field. As shown in Figures 2 and 4, the magnetic resistance characteristic of the ceramic superconductor relies on the value of the electric current flowing into the element. In other words, the greater this value, the greater the sensitivity.

With the M-type sensor, the narrow width of the electric current route presumably caused the increase in the effective density of electric current and furthermore in sensitivity. Second, the bulk element is considered to be different from the thick-film element produced by the spray pyrolysis method in terms of the magnetic resistance characteristics. In order to observe this difference--except for that produced by the configurational effect--the maximum increase rate $(\Delta\rho/\Delta B)$ max of each electric resistance rate P of the bulk element and the thick-film element, as a result of application of the magnetic field, is shown in Figure 6 as a function of the density of the electric current flowing into the element. The resistance rate ρ and the electric current density J were determined assuming that the electric current would flow uniformly into the element.

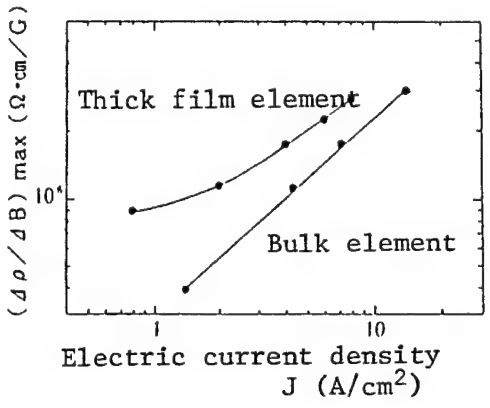

Figure 6. Comparison of Magnetic Resistance Characteristic of Bulk Element and Thick Film Element

Figure 6 tells us that an increase in the rate of the electric resistance of the thick-film element produced by the spray pyrolysis method is higher than that of the bulk element. The reasons for this higher increase rate are thought to be as follows:

1. The magnetic field can enter only into the finite depth from the surface of a superconductor by the Meissner effect. Accordingly, the magnetic field enters into most of the thick-film element produced by the spray pyrolysis method and this element effectively functions as a sensor. By contrast, only the surface and the immediate vicinity of the bulk element function as a sensor.

2. The bond strengths of the weak bonding conditions in the bulk element and the thick-film element are different

However, a detailed clarification of the above causes remains an issue for the future.

5. Application

It is expected that the superconducting magnetic resistance M-type sensor will be applied in many areas, thanks to its excellent features. The nondestructive detection of biological magnetism and material abnormality can be performed by detecting the weak magnetic field. This detection has been carried out primarily by the SQUID, which uses a metal-based superconductor. However, the SQUID requires very delicate construction and employs a complicated system technology called a flux lock loop. The configuration of the SQUID technology will be required in the future for ultrahigh sensitivity measurements such as magnetic brain waves. A superconducting magnetic resistance sensor whose element construction and system are simple can be expected to be applied in areas where there are great social needs, such as for detecting magnetic heart waves, magnetic lung fields, resources exploration, and the detection of abnormalities such as metal corrosion and fatigue, etc. Furthermore, with the progress in high-temperature superconducting materials, application of high-sensitivity magnetic sensors in areas where semiconductors and sensors of magnetic substances have been used can bring about unprecedented functional improvements. For example, if an ultrahigh magnetic head is realized using a superconducting magnetic resistance sensor, it will be possible to perform high-speed and high-density information readout. As noted above, we consider that the superconducting magnetic resistance sensor will contribute greatly to the advanced information society.

References

1. J. G. Bednorz and K. A. Muller. Z. Phys. B64, 189 (1986)

2. M. K. Wu, J. R. Ashburn, C. J. Torng, P. H. Hor, R. L. Meng, L. Geo, Z. J. Huang, Y. Q. Wang and C. W. Chu. Phys. Rev. Lett. 58, 908 (1987)

3. M. Kawai, T. Kawai, H. Masuhira and M. Takahasi. Jpn. J. Appl. Phys. 26, L1740 (1987)

4. S. Tsuchimoto, S. Kataoka, H. Nojima, R. Kita, M. Nagata, and H. Shintaku. IEDM Tech. Digest, IEEE, 867 (1987)

5. H. Nojima, S. Tsuchimoto and S. Kataoka. Article to be published in Jpn. J. Appl. Phys.

Fast Breeder Reactor Development Basic Strategy: Japan AEC Report

43062004 Tokyo GENSHIRYOKU SANGYO SHIMBUN in Japanese 2,8 Sep 88 pp 8,4

[2 Sep 88 p 8]

[Excerpt] The Japan Atomic Energy Commission's Expert Group on Fast Breeder Reactors (Hiroshi Murata, chairman) completed a report entitled "Advancing R&D on the Fast Breeder Reactor" on 26 August and submitted it to the commission. The report set a goal of the late 1990s to begin construction of an FBR experimental reactor and stressed the necessity of R&D so that FBRs will be able to compete economically with light-water reactors in practical applications. It also pointed out such things as the need to clarify the division of effort between the government and the private sector in regard to promotion of R&D. This newspaper will summarize the report in three installments beginning today.

Scenario for FBR Development

In deliberating policies on the progress of R&D, it is important to clarify the priority topics and R&D goals in each field of technology, based on a scenario running from the experimental reactor to practical reactors, which are the sites at which the successes of R&D are reflected and put to use. The development scenario up to the time of practical utilization is based on the long-term plan for the development and use of atomic energy, as follows.

(1) Opportunities will be established for successive construction of a number of reactors, each at the appropriate time, beginning with the demonstration reactor that will follow the "Monju" prototype reactor, with a goal of a practical utilization from the 2020s to about 2030.

R&D is to be implemented comprehensively from a long-term perspective, in such a way that there are practical prospects in each stage of construction.

(2) The electric power companies (Japan Atomic Power Company) are to take the leading role in the design, construction and operation of the experimental reactor, with appropriate cooperation from the government and the private sector. Construction is to begin in the latter half of the 1990s, and 1990 is the goal for selection of the fundamental method. The basic design and detailed design will follow that. In view of the development experience

accumulated so far in regard to reactor types, it appears that development will center on a sodium-cooled reactor using MOX fuel.

(3) To be practical, the FBR must be economical in the sense that it maintains standards of safety, reliability, and ease of operation and maintenance at least as high as those of the light-water reactor. With that objective, R&D is going forward on reducing the size and increasing the performance of plant equipment and facilities. The demonstration reactor that will follow the prototype reactor "Monju" has the status of the first stage in the long process of achieving practical application; it is to be developed as the reactor that makes it possible to look forward to practical application.

Structure for Promotion of R&D

With regard to the division of effort between the government and the private sector in FBR R&D, research related to the experimental reactor has already begun in the private sector, and private sector R&D will reach full force hereafter. Therefore, although it has not actually been established as a settled matter, it would be correct to say, as things now stand, that promotion of R&D in each sector will follow these lines:

Government: The private sector cannot be expected to carry out, by itself, the preliminary and fundamental R&D for practical use of FBRs, basic research including preparation of databases, or R&D that involves large development risks. The government will have responsibility for those things and for matters like safety regulations which are always the obligation of the government.

Private sector: R&D necessary for the design, construction and operation of plant beginning with the experimental stage is to be the responsibility of the private sector, as is R&D to improve safety, reliability and economy to practical levels.

During the development of the experimental reactor, there will be close contact between the Japan Atomic Power Company [JAPCO], which will play the leading role in design, construction and operation, and the Japan Power Reactor and Nuclear Fuel Development Corporation [PNC], which has played the central role in FBR R&D so far and which is expected to play an important role in future R&D as well. It is important that coordination be carried out within a structure of cooperation that also includes the Japan Atomic Energy Research Institute [JAERI], the Central Research Institute of Electric Power Industry [CRIEPI], and manufacturers, and that each entity pursue its responsibility in accordance with its own role. The FBR R&D Management Committee, a structure for cooperation that started up in 1986, is composed of JAPCO, PNC, JAERI and CRIEPI.

This committee was established, on the basis of the government's FBR development guidelines, to deliberate and coordinate the efficient division and management of the FBR R&D projects to be carried out by domestic entities, and of related international cooperation.

This activity is going smoothly at present, and it is appropriate that

concrete cooperation continue to go forward under this structure.

In particular, there has been technical cooperation between PNC and JAPCO to transfer the technology PNC has accumulated, and to develop the future experimental reactor. In promoting that cooperation it is important to continue a broad response that includes transfer of information, exchange of personnel and effective use of facilities.

R&D that Requires Large-scale Facilities

(1) Facilities in Japan, at PNC's Oarai Engineering Center, include the "Joyo" experimental reactor, fuel and materials irradiation test facility, and test facilities that deal with sodium, where fuel irradiation experiments are conducted and equipment for major components are developed. In addition, CRIEPI has large-scale facilities where research on earthquake-resistance has been conducted. In addition, there has been a variety of R&D using facilities in the United States and France.

In terms of efficiently carrying out the lengthy R&D needed to make the FBR practical, R&D that requires large-scale facilities is important from the aspect of fiscal planning as well. It is important that such R&D be conducted accurately and efficiently.

(2) To do this it will be necessary to respond to the future progress of development, such as the selection of the basic type of experimental reactor, including what sort of large-scale facility is necessary for what kind of research tasks, and how, concretely, the research will be carried out. At the same time it will be necessary to consider the sequence, so that results will be available when needed.

At that time it will be necessary to make effective use of the Oarai Engineering Center that has been prepared or is being prepared by PNC. Until then, it will be important to pay attention to the use of international cooperation.

It is therefore important to consider ideas in regard to a cooperative structure that includes PNC, JAPCO and the manufacturers, and the division of responsibilities among them.

(3) It is particularly important to take advantage of the experience of design, construction and operation of the prototype reactor "Monju," and thus ascertain the appropriateness of standards and analysis codes, improve performance, increase the longevity of fuel, verify the soundness of large-scale equipment and accumulate operation and maintenance data. And it is important to accurately use the results obtained for development of the experimental reactor and subsequent reactors.

International Cooperation

(1) To summarize the current state of international FBR R&D, experimental reactors have been developed in Europe through international cooperation among the major countries, but in the United States the Department of Energy and

others are hoping for Japanese cooperation in putting together the concept for a new type of FBR.

(2) Because Japan started on FBR R&D later than Europe and the United States, in advancing R&D, it has learned from the experience already gained by the countries of Europe and the United States, and emphasized the question of how to efficiently prepare, within Japan, the technological foundation for development of FBRs.

Moreover, there has been bilateral cooperation between Japan and the United States and multilateral cooperation among Japan, the United States and Europe or Japan and the countries of Europe on a number of the main technologies that make up FBRs. This cooperation has taken a number of forms, from exchanges of information and researchers to experimental research using large-scale facilities overseas. It will be necessary for Japan to continue these technology exchanges with the countries of Europe and the United States.

Figure: Japanese Fast Breeder Reactor Development

Fast Test Reactor "Joyo" (safety investigation 1969; construction permits 1969-73)

- Concept design: 1967-69
  - Facility permit application--1969
- Construction (design, fabrication, installation): 1970-75
  - Facility approval--Feb 1970
- Comprehensive function testing: 1975-77
  - Function testing begins--Jan 1975
- MK-I operation (breeder reactor core): 1977-81
  - First goes critical--Apr 1977
  - Reaches 50 MW--Jul 1978
  - Reaches 75 MW--Jul 1979
- Core transfer: 1982
  - MK-I operation ends--Jan 1982
- MK-II operation (irradiation reactor core): 1982 onward
  - MK-II goes critical--Nov 1982
  - Reaches 100 MW--Mar 1983

Prototype Reactor "Monju" (environmental studies etc. 1977-82; safety investigation 1980-83; construction permits 1984-87)

- Concept design & preliminary fabrication design: 1970-83
  - Construction site selected--Apr 1970
  - Environmental study begins--Aug 1978
  - Facility permit application--Dec 1980
    - Safety inspection begins--Dec 1980
- Construction (design, fabrication, installation): 1983-91
  - Facility approval--May 1983
  - Construction permit application--Dec 1984
- Comprehensive function testing: 1991-92
  - Equipment installation to be completed--Apr 1991
- Operation: 1992 onward

To go critical--Oct 1992

Test Reactor 1983 onward
Basic type selection: about 1990
Construction to begin: late 1990s

	MK-I	MK-II
Cumulative operation time	12,968 H	19,151 H
Cumulative thermal output	673,330 MWH	1,707,357 MWH
Maximum burn rate		
Pin maximum	40,500 MWd/t	61,000 MWd/t
Assembly average	40,100 MWd/t	55,000 MWd/t

[8 Sep 88 p 4]

[Excerpt] As previously reported, the JAECs Expert Group on Fast Breeder Reactors completed a report entitled "Advancing R&D on the Fast Breeder Reactor" on 26 August. The second installment of our series will introduce the situation surrounding FBR development.

Significance of FBR Development

The FBR is an epochal atomic reactor that produces more fuel than it consumes, as it is generating electric power. It is thought that, if plutonium comes to be fully used because of FBRs, demand for natural uranium will be greatly diminished and the problem of restricted supply of nuclear fuel sources for atomic reactors will be basically solved. Consequently, it will be necessary to promote development of FBRs as the major source of atomic power in Japan. In promoting that development, it is extremely important from the perspective of safety to actively construct a system for use of plutonium by FBRs that is superior to the system for use of uranium by light-water reactors.

Japan's active promotion of R&D from that perspective is not just a matter of strengthening the domestic energy supply base; it also has policy significance as a long-term contribution to the stable supply of energy for international society.

Moreover, because the technology for FBRs is integrated system technology that covers a very broad range of science and technology, promotion of this R&D will contribute to raising the level of a broad range of science and technology.

State of R&D in Japan

FBR development in Japan was begun on the basis of the JAEC's 1956 Long-term Plan for the Development and Use of Atomic Energy. In the first phase, basic research was implemented, primarily by JAERI. Then in 1966, JAEC set its "Basic Guidelines for Power Reactor Development" and made FBR development a national project, to be carried out with the cooperation of all sectors, crystallizing the full effort of the nation. PNC was established the following year as the organization charged with promotion. When PNC was established, the concept design of the "Joyo" experimental reactor and other

accomplishments of JAERI were transferred to it. Since then, PNC has been the focus for systematic implementation of R&D on basic technology, and it has pushed forward the development of the experimental reactor "Joyo" and the prototype reactor "Monju." Japanese power companies and manufacturers have participated in this national project by fabricating equipment and detailing personnel to PNC, and the accumulation of technology has grown steadily.

With a background of technology accumulated in work with light-water reactors, starting with their participation along with manufacturers in the Fermi Project in the United States from 1966 to 1972, the power companies carried out design research to streamline the design of the experimental reactor. The power companies, including CRIEPI, carried out various kinds of element research, accumulating technology of their own. And in the course of cooperation on construction of the prototype reactor "Monju," they managed the technical cooperation and construction work, and gained practical experience. In the 1987 Long-term Plan for the Development and Use of Atomic Energy, it is made clear that the power companies are to be the main force in the design, construction and operation of the demonstration reactor that is to follow the prototype reactor. The power companies have entrusted the business of the demonstration reactor to JAPCO.

The FBR R&D Management Committee, composed of JAPCO, PNC, JAERI, and CRIEPI, has done the necessary consultation and coordination for the implementation of R&D for development of the demonstration reactor and has promoted it smoothly and efficiently.

Other matters involved in making FBRs practical include seismic experiments, other technology verification experiments, and feasibility studies for major equipment, all of which have received government support.

Looking at the state of research on the nuclear fuel cycle, R&D on FBR reprocessing technology has been carried out in PNC. Japan is now at the stage of designing facilities capable of experiments on the engineering scale (recycling equipment test facility).

It has been decided that construction plans for a pilot plant, to begin operations in the 21st century, will be fleshed out with full consideration given to the results mentioned above.

PNC is also doing research on MOX fuel processing technology. The Plutonium Fuel Production Facility (PFPF) completed its FBR line in 1987, and operations were to begin in 1988.

The state of R&D by the major entities concerned are indicated below.

The Power Reactor and Nuclear Fuel Development Corporation

Since its establishment in October 1986, PNC has advanced development of an experimental reactor, then a prototype reactor, based on the fundamental government policy of developing an FBR using autonomous technology. Because such development requires R&D in a broad range of fields, R&D facilities including the Oarai Engineering Center were furnished, and R&D was done first

for the "Joyo" experimental reactor, and then for the "Monju" prototype reactor. The "Joyo" first went critical in April 1977, and an experiment in which it was operated as the core of an FBR with a thermal power of 50,000 KW began in October 1987 [as published]. It was subsequently converted to an irradiation core, and various experiments including irradiation of fuel and materials with a thermal output of 100,000 KW have been conducted since March 1983.

Facilities approval for the "Monju" prototype reactor was received in May 1983, and full-scale construction work began in October 1985. Construction is going forward now with criticality predicted in October 1992.

In addition to R&D involved in the construction and operation of the experimental reactor "Joyo" and the prototype reactor "Monju," PNC has improved the level of core and fuel design, high-temperature structural design methods and methods for analysis of reactor behavior in the event of a malfunction. It has also raised the level of fundamental element technology for large reactors and conducted design research in that connection, and thus established and enhanced basic technology for achieving a practical FBR.

Japan Atomic Power Company

The electric power companies began preparatory design research for a large, practical reactor in the latter half of the 1970s. In their "Research on FBR Demonstration Reactor Concepts" of FY 1981-83, they conducted studies to improve the safety, feasibility, operability, maintainability and economy of the major systems of a tank-type reactor, and of all systems for a loop-type reactor, with reference to the prototype reactor "Monju." It was consequently estimated that construction costs for a one million KW reactor would be three to four times those of a light-water reactor and recognized that costs would have to be cut deeply. "Rationalized design research" to find cost-cutting measures began in 1984.

The power companies entrusted the work of FBR R&D to JAPCO. Since 1986 JAPCO has performed, as a part of its demonstration reactor design research, "research to point out innovative technology and effect rationalization" by studying the feasibility of innovative technology and the effect of cost reductions that can be adopted in the stage of practical application, as well as R&D necessary to smoothly advance basic type selection as a key element of experimental reactor construction, and design, construction, operation and maintenance considerations. It has also carried out R&D to improve safety and reliability in preparation for practical application, and to improve economy.

Japan Atomic Energy Research Institute

Making use of its potential for a broad range of atomic energy research, JAERI has for the most part conducted basic research. In connection with fuel and materials, it has surveyed carbonized fuels and done irradiation experiments with JRR-2 and JMTR. It has also performed neutron physics research on physical construction and shielding of reactors using FAC, and research to evaluate nuclear data. It has examined safety research including fuel damage experiments using NSRR.

Central Research Institute of Electric Power Industry

CRIEPI, taking advantage of the technology it has accumulated as the central laboratory of the power companies, has conducted research since 1984 to reduce FBR costs by improving designs of earthquake-resistant structures, streamlining equipment design, improving high-temperature structural design methods to improve structural reliability, and rationalizing heat-flow design. It has also examined innovative technology that will contribute to practical application of FBRs.

Figure: World Fast Breeder Reactor Development

Country	Type	Name	Const. begun	First critical	Opns. begun	Closed
France	experimental	Rhapsodie	1962	1967	1967	1983
(1)	prototype	Phoenix	1986	1973	1974	
	demonstration	Superphoenix	1977	1985	1986	
Britain	experimental	DFR	1955	1959	1963	1977
(1)	protonype	PFR	1966	1974	1976	
W.Germany	experimental	KNK-II	1975	1977	1979	
(1)	prototype	SNR-300	1973			
Italy (1)	experimental	PEC	1976			
U.S.	experimental	Clementine	1946	1946	1946	1953
	experimental	EBR-I	1946	1951	1951	1963
	experimental	EBR-II	1957	1963	1965	
	experimental	Fermi	1956	1963	1966	1971
	experimental	SEFOR	1965	1969	1969	(1971)
(2)	experimental	FFTF	1970	1980	1980	
USSR	experimental	BR-10 (BR-5)	1971	1973	1973	
	experimental	BOR-60	1965	1969	1971	
	prototype	BN-350	1965	1972	1973	
	prototype	BN-600	1971	1980	1981	
(3)	demonstration	BN800	1987			
India	experimental	FBTR	1972	1985	1985	
Japan	experimental	Joyo	1970	1977	1977	
	prototype	Monju	1985			
	demonstration (4)					

(1) EFR Project (2) LMR Project (3) BN-1600
(4) Demonstration Reactor Project

Source: "Status of Liquid Metal Cooled Fast Breeder Reactors" (IAEA Tech. Report No. 246)

Superconductivity Technology Patents Reviewed (III)

43067017 Tokyo KINO ZAIRYO in Japanese Oct 88 pp 57-70

[Article by Tohru Kodoh of the company Japan Association of Consulting Engineers]

[Text] **1. Introduction**

Progress has been made in the application of superconductivity technology to electric power systems, including various types of power equipment, superconductive generators, superconductive power transmission, power storage, and so on. It will become possible to create strong magnetic fields and enable large electric currents by obtaining high current densities with very low losses. In connection with the progress of R&D in oxide system materials (wire formation, increased current density, explication of magnetic phenomena, formation of long wires, and formation of magnets) especially, such things as improved efficiency, simplification of facilities, conservation of energy, and conservation of resources are becoming clearer.

Under MITI's basic plan "Superconductive Power Applications Technology," R&D goals and content have been formulated for the 8 years beginning in 1988,[1] as shown in reference Figure A.

2. Superconductive Power Generation (Superconductive generators, MHD power, nuclear fusion power, etc.)

2.1. Superconductive Generators[2,4]

(1) A superconductive synchronous machine characterized by an increase of flux linkage with the armature winding and heightened flux density of the armature winding achieved through the complete diamagnetic effect in superconductive parts of leakage flux produced in magnetic windings (Patent granted No 61-14749: Kansai Electric Power Co.) (Figure 1).

(2) A magnetic field winding device characterized by a superconductive field winding divided into a number of sectional windings of positive and negative polarity facing each other across an armature axis in the permanent magnet rotation mode, such that a closed circuit is formed between the sectional windings. This provides the benefits of both the series method

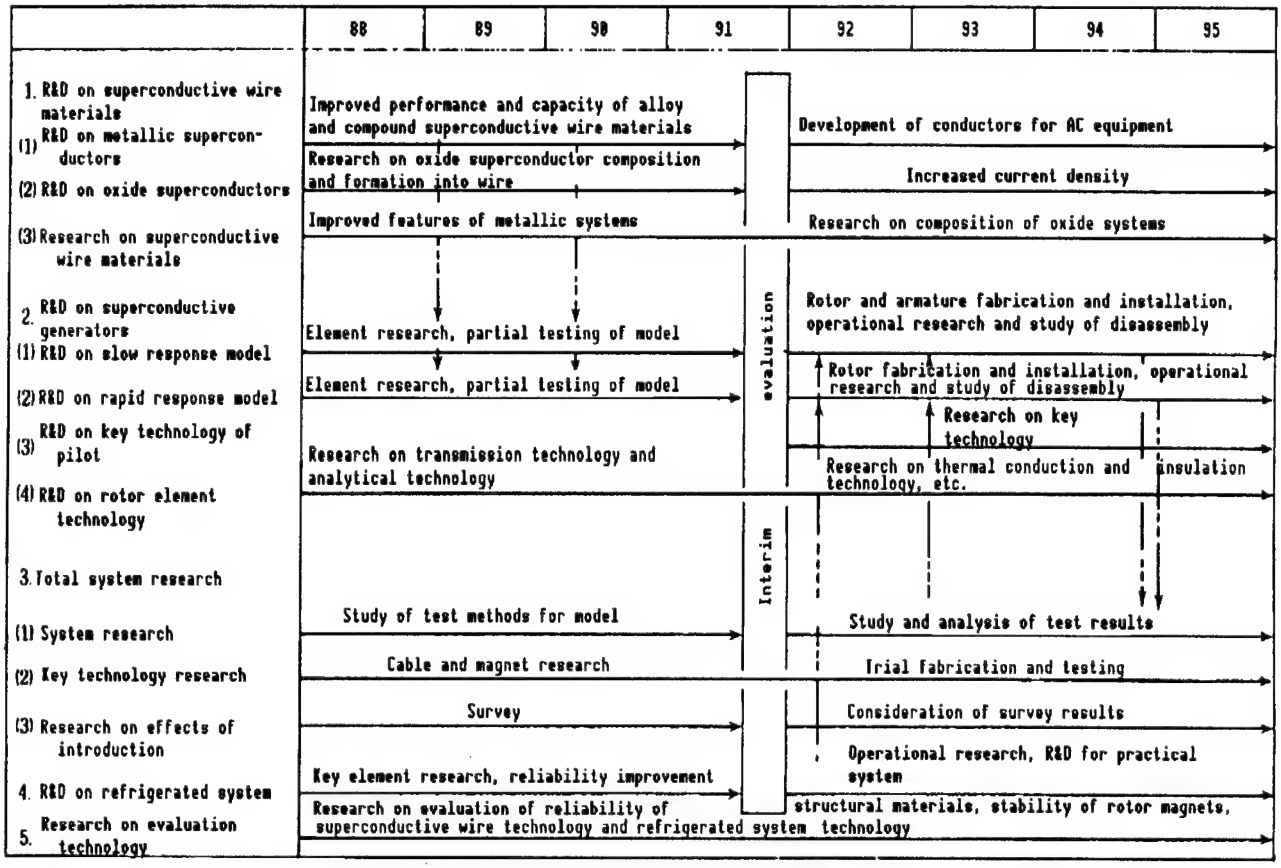

Reference Figure A: Basic Plan "Superconductive Power Applications Technology" for Large-Scale Energy Conservation Technology R&D

Summary of Plan

(1) Development of alloy and metallic compound conductors that can be used in superconductive power equipment
(2) Oxide system wire formation and current density improvement needed for application to power equipment
(3) 200 MW pilot equipment (for verification of technology) pertinent to prototype and practical equipment
(4) 70 MW model (for R&D) equipment
(5) R&D on total system, refrigerated system and evaluation technology

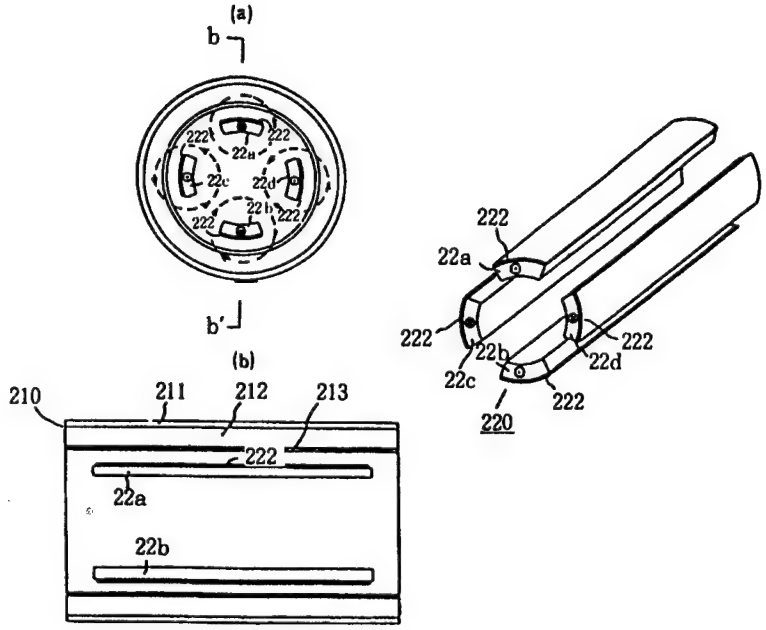

Figure 1.

Key: 210: Stator
211: External shielding
212: Armature winding
220: Rotor
22a-22d: Field winding
222: Superconductive parts

and the independent closed circuit method, and avoids dielectric and magnetic damage to the rotor (Patent granted No 62-55932: Toshiba Corp.) (Figure 2).

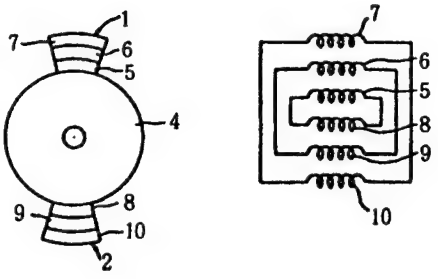

Figure 2.

Key: 1,2: Superconductive field winding
4: Rotor
5-7: Sectional winding
8-10: Sectional winding

(3) A superconductive rotor characterized by inner damper shielding divided for the full length in the axial direction into a number of pieces equal to the number of field poles, with the sections electrically insulated from

each other and placed between the magnetic poles of the field. This enables superior damping and electromagnetic shielding, and reduces the stress generated in the inner damper shielding (Patent granted No 62-55391: Hitachi, Ltd.) (Figure 3).

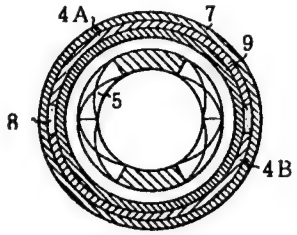

Figure 3.

Key: 3: Outer damper shielding
4A, 4B: Inner damper shielding
5: Superconductive field winding
7, 9: Reinforced cylinder
8: Insulation

(4) A high pole-load superconductive generator in which a superconductive coil wrapped with high critical-field superconductive wire is applied to the portion near the magnetic pole. As a result, the compound superconductive coil is small and easily wound, reliability is high and the overall cost of rotor fabrication is low (Patent granted No 62-55393: Mitsubishi Electric Corp.) (Figure 4).

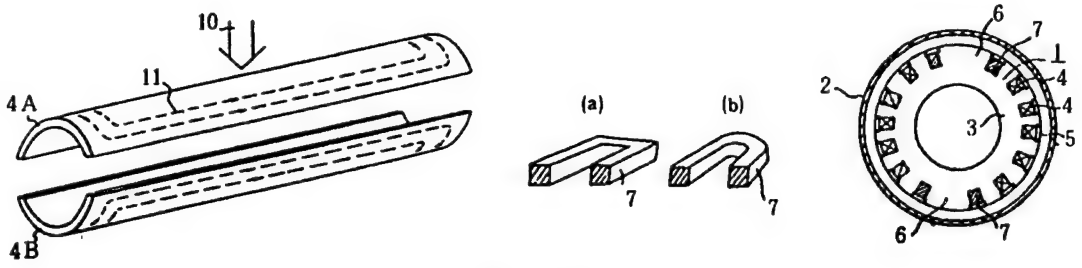

Figure 4.

Key: 1: Rotor
3: Coil attachment axis
4: Nb-Ti superconductive coil
6: Magnetic pole
7: Compound superconductive coil

(5) A very low temperature coolant feed and discharge device for a superconductive rotary machine, characterized by improvement of the tip of the rotor axis. That is, this invention can effectively isolate internal heat transmission and heat penetration from the outside. Because of its simple structure, it makes very economical superconductive rotary machines practical (Patent granted No 62-3664: Fuji Electric Co.) (Figure 5).

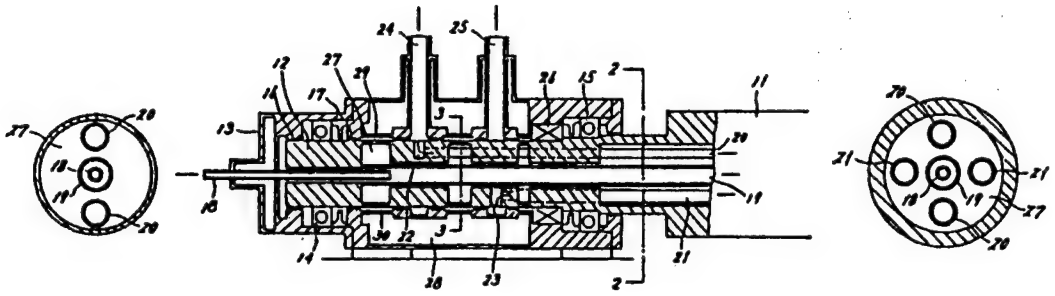

Figure 5.

Key: 12: Cylindrical part
13: Housing
18: Coolant injection pipe
19: Coolant feed pump
20, 21: Gas recovery pipe
22, 23: Access hole
24, 25: Gas discharge port

(6) A superconductive rotor cooling device in which the coolant flow that has passed through the field winding contributes to the cooling of the low-temperature shield so as to enable a relatively rapid cooling response to the variable thermal load that occurs in the low-temperature shield (Patent granted No 62-17472: Siemens) (Figure 6).

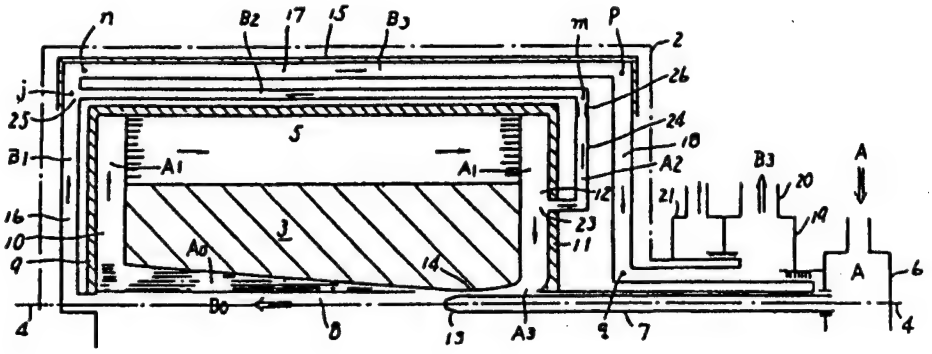

Figure 6.

Key: A: Supply coolant
A1: 1st supply coolant flow
B1: 2d supply coolant flow
A2,B2,A3: Partial flow
5: Superconductive field winding
7, 10: Supply pipe
8: Mixing chamber
9, 11: End wall
12: Discharge pipe
13: Spray nozzle
14: Absorption trough
24: Connecting pipe
26: Compression section

(7) A superconductive generator characterized by a radiation shield function to minimize the possibility of mechanical disequilibrium caused by a serious accident or other operational abnormality (Patent application published No 59-226654: Westinghouse) (Figure 7).

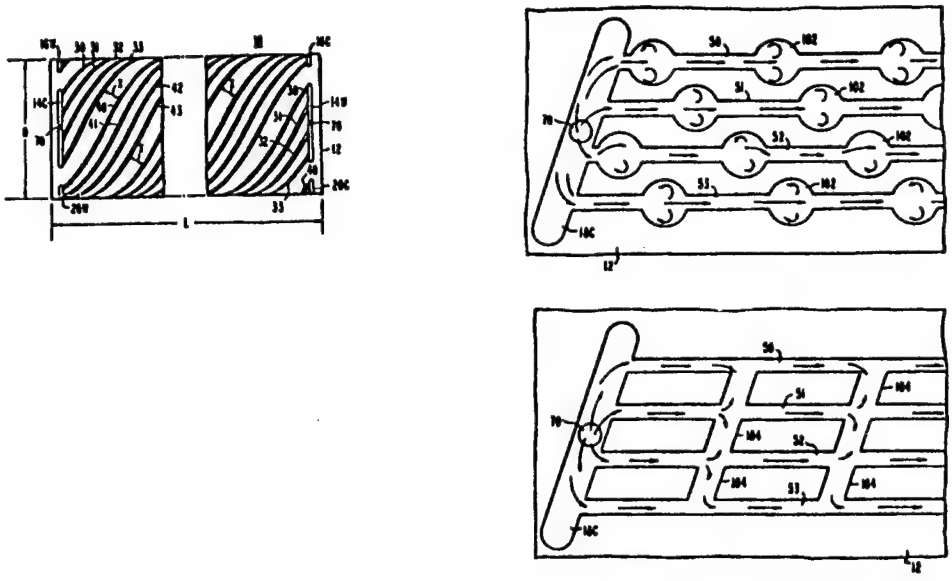

Figure 7.

Key:		
	10:	Radiation cover
	12:	Inner cylinder
	14C,16C,18C,20C:	Cold outward fluid channel
	14W,16W,18W,20W:	Warm outward fluid channel
	30-33,40-43,50-53,60-63:	Spiral fluid channel
	70:	Diametric fluid channel
	102:	No connection
	104:	Fluid channel connector

(8) A stator for electrical machinery having superconductive, three-phase windings including a tubular part and end plates that form a very low temperature space, additional tubes, and the winding (Patent application published No 62-181667: ARUSUTOMU) (Figure 8).

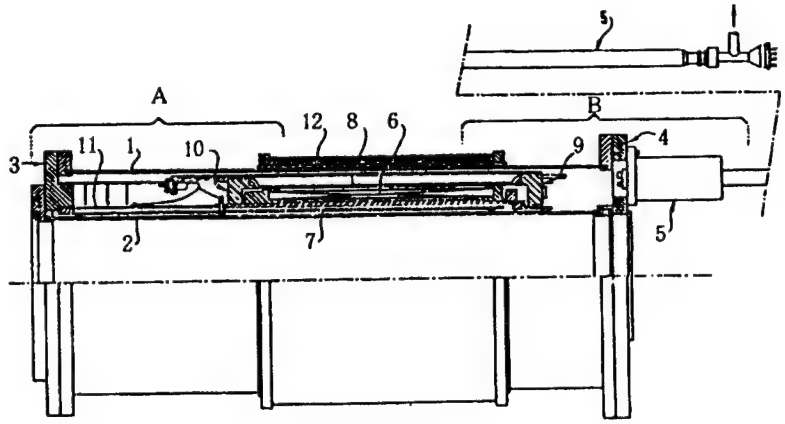

Figure 8.

Key:				
	1, 2:	Cylinder	7, 8:	Tube
	3, 4:	Terminal plate	9, 10:	Terminal plate
	3:	Current lead	11:	Support tube
	6:	Superconductive winding		

2.2 MHD Power Generation[3,8]

In MHD [magneto hydrodynamic] power generation, which uses high-temperature gas (plasma, combustion gas, fluid metal) electromagnetic fluids, power turbines are turned with high efficiency by plasma gases, etc., accelerated by superconductive coils. The principle of MHD power generation is shown in reference Figure B.[3] In Japan this was adopted in 1978 as a large project on energy conservation technology, as a part of the Moonlight Project. More recently, the Electrotechnical Laboratory succeeded in generating 500 kw. The success of R&D on the major components and parts of MHD technology (gas burners, refractory materials, superconductive magnets) has great significance in processes that form the foundation of superconductivity technology. The superconductive magnet technology in particular has been praised for its great ripple effect on R&D regarding such things as high-energy physics, nuclear fusion, and the linear motorcar. Reference Figure C shows the structure of a superconductive magnet for MHD power generation.[8] This magnet is produced in the United States; it has 210 MJ regenerative energy (the maximum value for MHD), and a maximum magnetic field of 6.9 T.

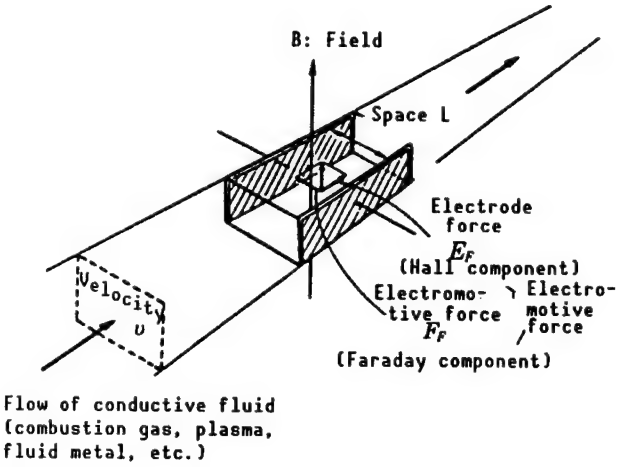

Reference Figure B: Principle of MHD Power Generation[3]

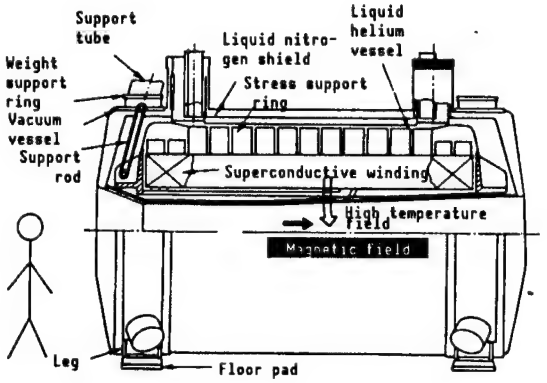

Reference Figure C: Structure of Superconductive Magnet for MHD Power Generation[8]

The protective devices of conventional high-voltage power sources have been liable to cause severe damage to such systems as the power supply system and control system (or human engineering system). To reduce that danger, a device to effectively block damage to or destruction of superconductive magnets and other equipment has been proposed. By using the rotary machine as an emission load for stored energy, it would prevent the occurrence of abnormally high voltages during conductive transfer, and rapidly convert stored energy into another form of energy (Patent application published No 58-97806: AIST Electrotechnical Laboratory) (Figure 9).

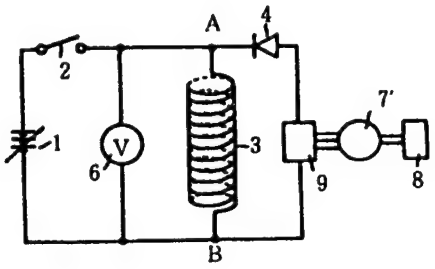

Figure 9.

Key: 1: Power supply
2, 10: Switch
3: Superconductive magnet
4: Diode
5: Protective resistance
6: Voltage detector
7: Rotary machine
8: Mechanical load
9: DC/AC transducer

Depending on the type of load device, this invention can convert and recover rotational energy as electromechanical energy, mechanical energy, chemical energy, thermal energy, or other useful forms of energy. This advantage is not part of the conventional protective function.

2.3 Nuclear Fusion Power Generation[5]

(1) A toroidal field coil with improved structure of welds in the reinforced frame, constituted such that the side reinforced frame and the inner and outer reinforced frame can be welded together without leaving unwelded portions (Patent granted No 62-53927: Hitachi, Ltd.) (Figure 10).

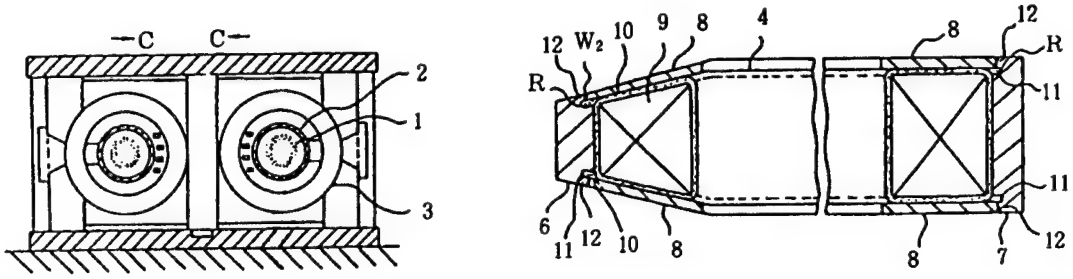

Figure 10.

Key: 1: Plasma
2: Vacuum vessel
3: Toroidal field coil
4: Coil
5: Reinforced frame
6: Inner reinforced frame
7: Outer reinforced frame
8: Side reinforced frame
9: Coil conductor
11: Slot
12: Projection
13: Cooling tube

(2) A small, highly reliable, high-performance nuclear fusion device in which a leaf of semiconductor material is inserted between leaves of insulator material, the impedance of the insulator layer of the collector plate is reduced and the creeping breakdown voltage is increased (Patent granted No 62-46964: Toshiba Corp.) (Figure 11).

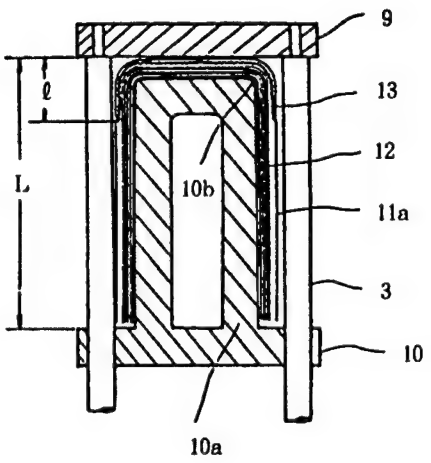

Figure 11

Key: 1: Coil device
2: Collector plate
3: Coaxial cable
9: High voltage collector plate
10: Low voltage collector plate
10a: Opposing electrode
12: Polyethylene film insulator layer
13: Semiconductor plastic film layer

(3) A method of fabricating superconductive wire material with markedly improved Jc, in a strong field of at least 14T, and Hc_2, in order to eliminate the defects of conventional Mb_3Sn superconductive wire. The fields of application include those which demand large, strong-field magnets, such as nuclear fusion reactors, high energy physics, and energy storage (Patent application published No 62-109953: STA National Research Institute for Metals) (Table 1).

Table 1.

Sample No	Heat treatment (°C × min.)	Ti concentration in Sn bath (%)	Cn concentration in Sn bath (%)	Ic (16T) (A)	over all Jc (16T) ($\times 10^4 A/cm^2$)
1	950 × 15	0	0	55	1.60
2	900 × 15	0	5.0	67	1.90
3	950 × 15	2.5	0	118	3.50
4	950 × 15	5.0	0	140	4.10
5	900 × 15	2.5	5.0	136	3.95
6	900 × 15	5.0	5.0	147	4.25

(4) A superconductive magnet wire material made of a new alloy (V-Ti-Ta) suited to use at superfluid helium temperatures, and a method of fabricating it. It can be used in various strong-field magnet applications, including nuclear fusion reactors, particle accelerators, energy storage, and linear motorcars (Patent granted No 60-54379: STA National Research Institute for Metals).

(5) A rotating field flux pump device that meets the requirements for use in high-efficiency pumps. A device in which a number of superconductive pumps can be connected in series in the direction of conduction, such that each rotation of the rotating field will cause many pump operations in a flux pump that excites a superconductive magnet in a nuclear fusion reactor plasma device (Patent granted No 59-51726: National Railways, Toshiba Corp.) (Figure 12).

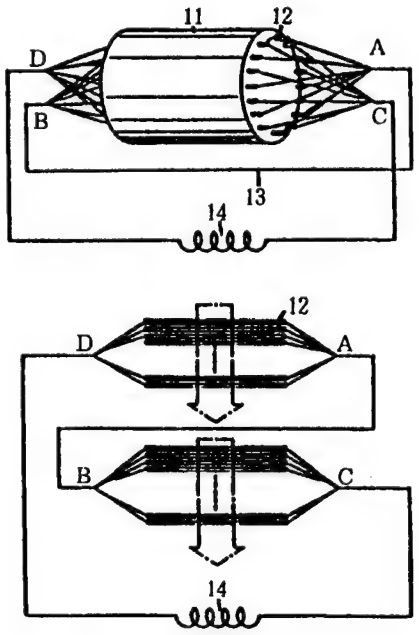

Figure 12.

Key: 11: Core (source of rotating field
12: Superconductive wire (superconductive pump)
13: Lead wire (series connection wire)
14: Superconductive coil

(6) A superconductive with simple structure and connections that have high stability and reliability, both electrically and mechanically, for use in the superconductive coil of a nuclear fusion device (Patent granted No 62-19022: Japan Atomic Energy Research Institute, Hitachi, Ltd.) (Figure 13).

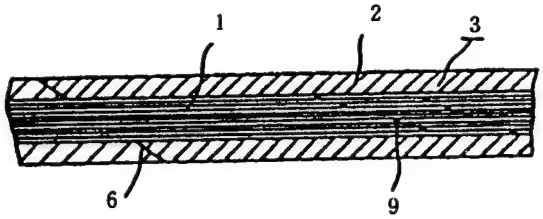

Figure 13.

Key: 1: Superconductive strand
2: Stable material
3: Superconductive conductor
6: Stable material connection
9: Superconductive strand connection

(7) A toroidal coil that forms a toroidal field laid out in the shape of a torus. It is possible, using this invention, to chamfer the coil conductor widthwise, and thus produce a high-precision toroidal coil by reducing the effect of "warping" due to bending of the superconductor (Patent granted No 62-8922: Japan Atomic Energy Research Institute, Mitsubishi Electric Corp.) (Figure 14).

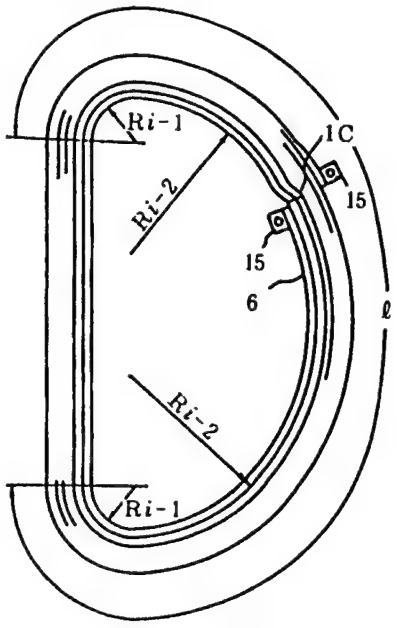

Figure 14.

Key: 1: Toroidal coil
6: Coil conductor
C: Chamfer

(8) A large superconductive coil and support structure that has a field in the gigaJoule range, involving compact nuclear fusion equipment (coil, cryostat, and cooling system) (Patent granted No 59-28968: Japan Atomic Energy Research Institute, Mitsubishi Electric Corp.) (Figure 15).

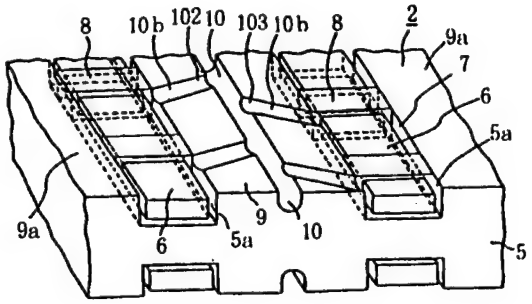

Figure 15.

Key:
1: Superconductive coil
2: Superconductive disk
5: Holder
6: Superconductive wire
9: Tooth of holder
10: Channel for cooling medium
10a, 10b: Branch channel
100-103: Branch channel opening

(9) A device that confines high-temperature plasma by means of a double helical field generated by a helical coil wrapped around the outer wall of a toroidal discharge tube. That is, a device that makes practical the steady operation of a stellerator, helotron, torsatron or other nuclear fusion reactor (Patent application published No 60-263408: Kobe Steel, Ltd.) (Figure 16).

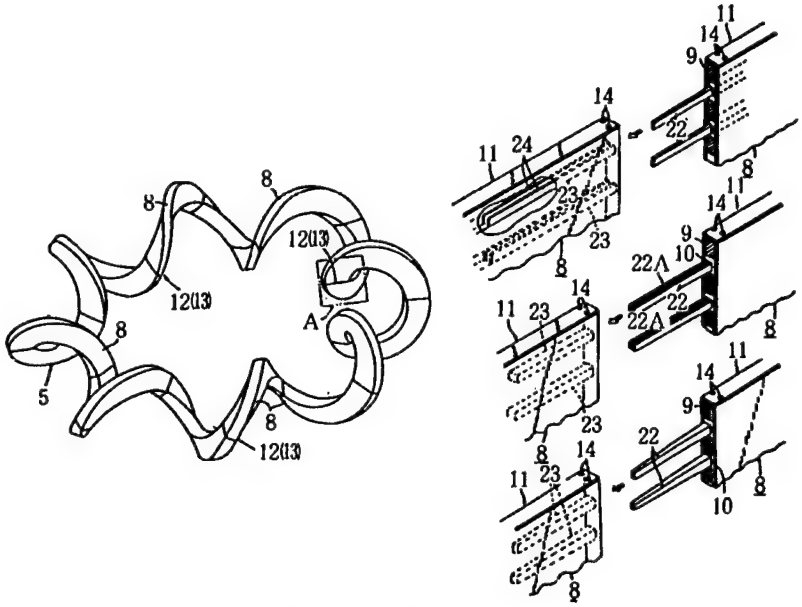

Figure 16.

Key: 5: Helical coil
8: Module coil
10: Superconductive coil
12 (13): Male/female fitting

(10) An Nb_3Sn very fine multicore compound superconductive magnet for a strong-field generating device to be used in nuclear fusion reactor research (Patent application published No 61-174366: Sumitomo Electric Industries) (Figure 17).

(11) Superconductive wire cooled by forced recycling of the cooling medium (Patent application published No 58-162008: AIST, Fujikura, Ltd.) (Figure 18).

(12) A method and device to improve flux, residual bubbles, and adhesion strength, and to resolve the most serious distortions in using Nb_3Sn or other alloy superconductive wires in a compound conductor (Patent granted No 61-16136: Showa Electric Wire & Cable Co.) (Figure 19).

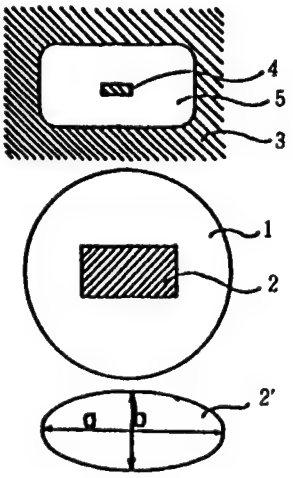

Figure 17.

Key:
1: Ingot of CuSn alloy
2,2': Bar of Nb
3: CuSn portion
4: Nb portion
5: Nb_3Sn layer

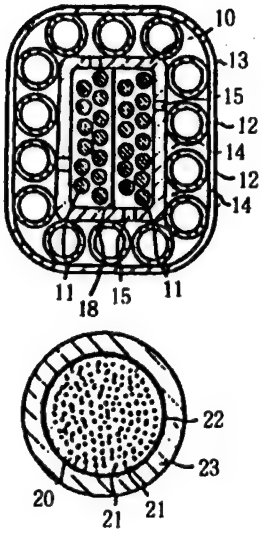

Figure 18.

Key:
10: Stabilizing material
11: Superconductive strand
12: Spacer
13: Outer sheathing
14: Coolant channel
15: Connecting channel
16: Space between superconductive strands

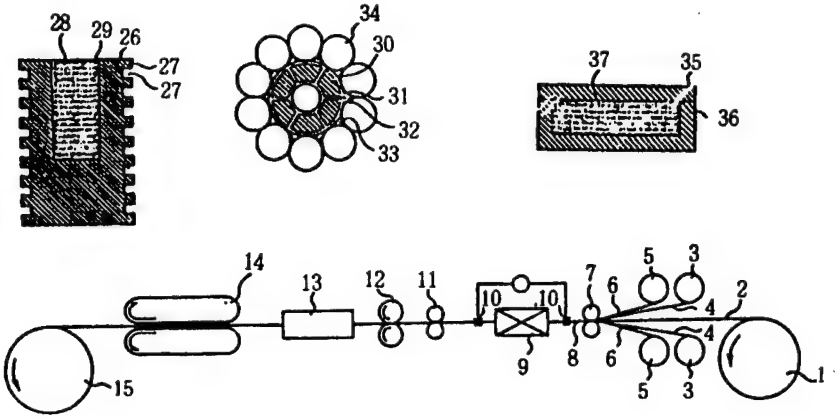

Figure 19.

Key:
1,3,5: Conveyor mechanism
2: Superconductor
4: Low melting point alloy tape
6: Stabilizing material
7,11: Shaping roller
8: Compound superconductor
9: Split high frequency heating device
10: Ultrasonic oscillator
12: Metallic rotating flange
13: Cooling tank
14: Endless rail traction mechanism
15: Winding mechanism

3. Superconductive Power Transmission (Direct current transmission, energy transmission underground transmission cable)[6]

(1) A power supply device (DC-AC-DC conversion) that effectively supplies coil energy from a superconductive energy storage coil by using an L-C parallel resonant tank circuit for commutation voltage generation in place of the commutation condenser, in order to supply an intermittent load from nuclear fusion (Patent granted No 62-33823: Mitsubishi Electric Corp.) (Figure 20).

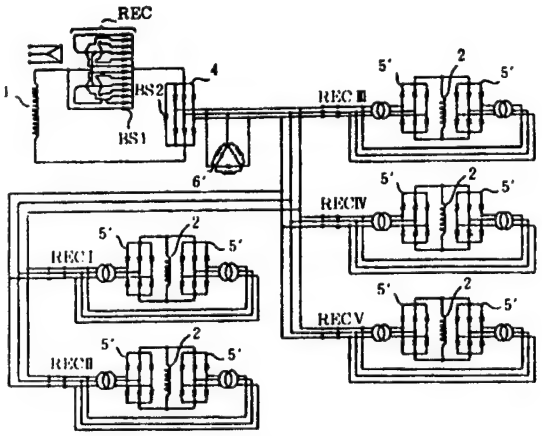

Figure 20.

Key: 1: Coil for superconductive energy storage
2: Storage coil charging circuit
4: Inverter
5': Rectifier
6': L-C parallel resonant tank circuit for commutation voltage generation

(2) A method to increase cooling capability by covering the surface of the conductor that contacts the liquid helium coolant with a thin film of metal (or metallic compound) having a higher thermal resistance than the conductor surface, thus contributing greatly to reduction of the cost of the entire system, including reduction of the size of superconductive magnets, reducing the amount of superconductive material and reducing the cooling volume. This method can be applied to compound superconductors used in superconductive power cables and various superconductive magnets (Patent granted No 62-33822: Mitsubishi Electric Corp.) (Figure 21).

(3) A compound superconductor characterized by covering the surface of the conductor in contact with liquid helium, the coolant, with a thin film of metal (or metallic compound) having a higher thermal resistance than the material of the surface (to enhance cooling capability) (Patent granted No 62-17809: Hitachi Cable, Ltd.) (Figure 22).

(4) A reverse-twist device capable of easily varying the angle of twist of shield wires to the right or left in a cable with alternating reverse twist shield wires (Patent application published No 62-172608: Hitachi Cable, Ltd.) (Figure 23).

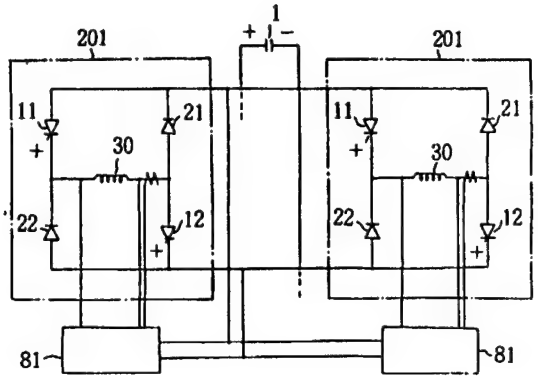

Figure 21.

Key:
- 1: Condenser
- 11, 12: Self-operating switch
- 21, 22: Diode
- 61, 62: Diode
- 30: Coil
- 81, 82: Flow control circuit
- 91: Switching circuit
- 101-104: Reverse conducting thyristor
- 111-114: Reverse conducting thyristor
- 121-124: Commutation condenser
- 131-134: Commutation reactor
- 201: Bidirectional energy transmission circuit in which coil current is constant
- 301: Bidirectional energy transmission circuit in which coil current is reversible
- 401: Energy transmission circuit for energy emission
- 402: Energy transmission circuit for energy absorption

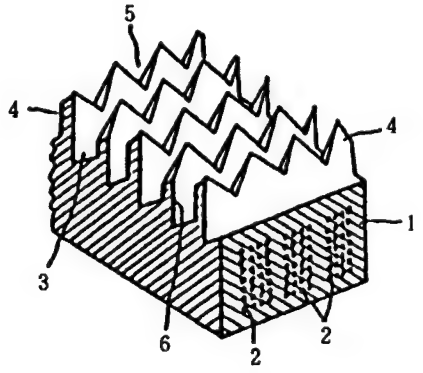

Figure 22.

Key:
- 1: Normal conductor
- 2: Superconductor
- 3: Trough
- 4: Projection
- 5: Break
- 6: Thin film

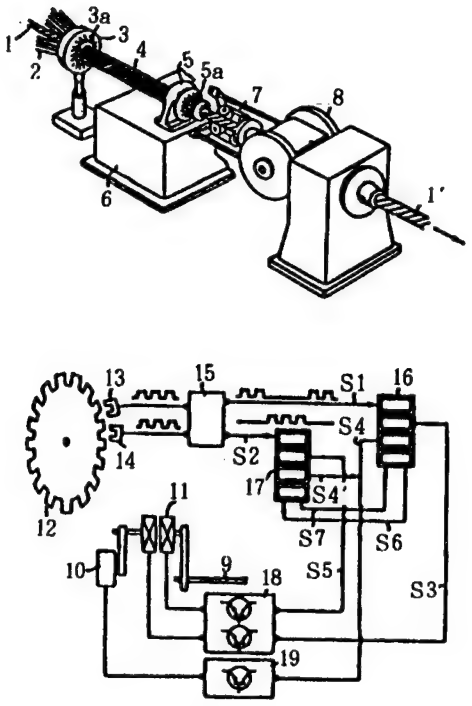

Figure 23.

Key: 1: Cable
2: Shield wires
5: Reversing head
10: Break
11: Reversing clutch
15: Rotation information detector
(16-19: Means of controlling break and reversing clutch)
16: Regular-twist mechanism
17: Reverse-twist mechanism
18, 19: No-contact controller

(5) A method of fabricating superconductive coaxial cable, intended to reduce transmission losses based on regular variations in the inside diameter of the outer conductor, and to prevent amplification of transmission losses caused by multiple reflection at certain frequencies (Patent granted No 58-1487: Fujikura, Ltd.) (Figure 24).

(6) Superconductors made of compounds like Nb_3Sn and V_3Ga exhibit superconductivity at temperatures of about 15 K to 18 K. Because it is not economical to cool with expensive liquid helium, this invention makes it possible to reach low temperatures in the 13 to 20 K range necessary for superconductivity in compound superconductors by using liquid nitrogen, which is less expensive. The invention is a superconductive cable line that can also be used for transport of liquid gases (Patent granted No 57-7444: Showa Electric Cable & Wire Co.) (Figure 25).

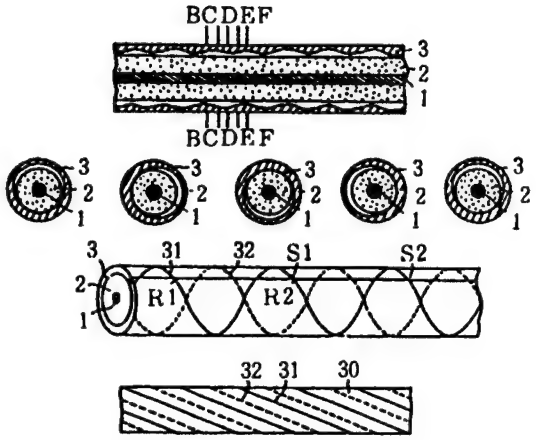

Figure 24.
Key:
1: Core conductor
2: Insulator
3: Outer conductor
4: Pressure roller
5: Mold
30: Tape for outer conductor
31: Peak portion
32: Trough portion

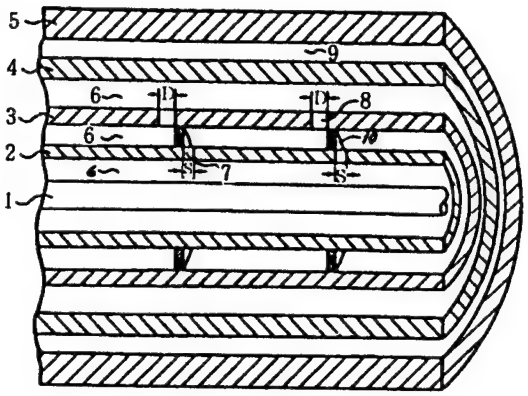

Figure 25.
Key:
1: Superconductive cable
2: Cable conduit
3: Cooling conduit
4: Reduced pressure conduit
5: Adiabatic conduit
6: Hydrogen
7, 8: Opening
9: Nitrogen
10: Partition strip

4. Power Storage and Supply Stabilization Systems[7]

(1) An electromagnetic energy storage device characterized by provision of multiple transformers electrically connected to superconductive coils and AC/DC transducers (or interconnected in series) (Patent application published No 59-188982: Toshiba Corp.) (Figure 26).

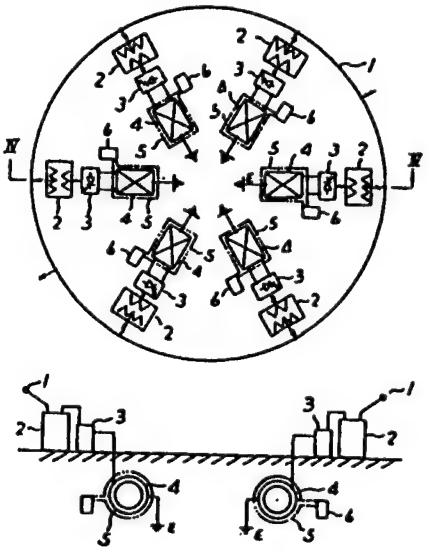

Figure 26:
Key:
1: Power line
2: Transformer
3: Transducer
4: Superconductive coil
5: Vacuum vessel
6: Cooling mechanism
7: Impedance element

(2) A superconductive device capable of protective action without power losses, in which multiple sets of superconductive units are operated so that if one superconductive unit does malfunction, its stored energy is transferred to other, sound superconductive units (Patent application published No 61-119802: Hitachi, Ltd.) (Figure 27).

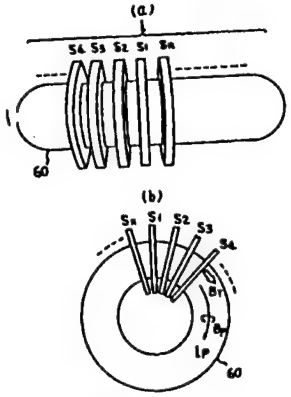

Figure 27.

Key:
1:	Superconductive device
2:	Control mechanism
3:	Cooling mechanism
60:	Vessel
A:	Power system
G:	Generator
Sc1-SCn:	Superconductive coil
T1-Tn	AC/DC transducer
V1-Vn	Valve
e1-en	Transducer forward/reverse switching circuit

(3) A superconductive power storage magnet that requires minimum space in the electromagnetic power support structure, so that it is possible to facilitate assembly and maintenance of superconductive magnets in the support structure, and to give the framework the shape that is optimal for response to stress (Patent application published No 59-18617: Tokyo Electric Power Co., Mitsubishi Electric Corp.) (Figure 28).

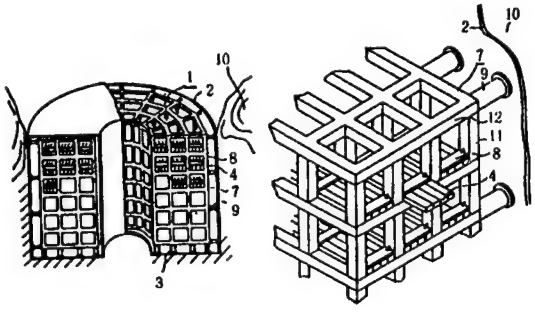

Figure 28.

Key:
1:	Superconductive magnet	7:	Framework structure
2:	Vessel	11:	Axial support
4:	Superconductive cable	12:	Diametric support

(4) An energy storage device (protective permanent current switches connected in parallel) in which electrical energy is passed through a thyristor transducer to convert it from alternating current to direct current, then stored in a superconductive magnet (Patent application published No 60-5744: Fuji Electric Co.) (Figure 29).

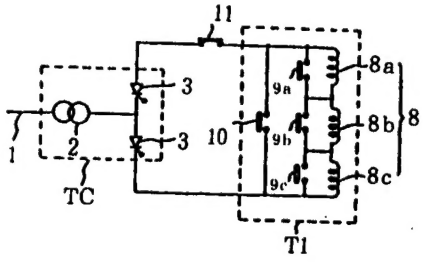

Figure 29.

Key: 8: Superconductive magnet
8a,8b,8c: Superconductive coil
91,9b,9c: Protective permanent current switch
11, 12: Switch
TC: Thyristor converter
T1, T2: Cryogenic tank

(5) Energy transfer circuitry for a superconductive energy accumulation device, in which a circuit with resistance and a thyristor in series is inserted in parallel with a superconductive load coil, such that the thyristor can be controlled to ignite when the current of the superconductive load coil is 0 or below a set value. It is then possible to steadily transfer energy to the superconductive load coil even when the load coil current is 0. Moreover, it is possible to reduce energy losses from the loaded resistance to the extent that they can be ignored. (Patent granted No 59-27171: Fuji Electric Co.) (Figure 30).

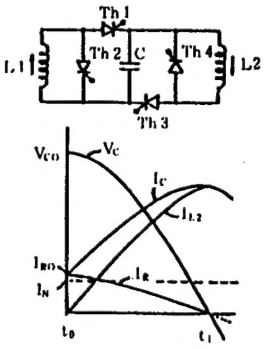

Figure 30.

Key: L1: 1st superconductive coil
L2: 2d superconductive coil
Th1-Th5: Thyristor
R: Resistance

(6) Terminal parts (using plastic busing cones) for power supply conductors used in cryogenic equipment such as superconductive magnets and very low temperature cables, including low-temperature/low-resistance cables and superconductive cables, to be located in both cryogenic and normal-temperature areas (Patent granted No 58-55730: Dainichi Nippon Densen) (Figure 31).

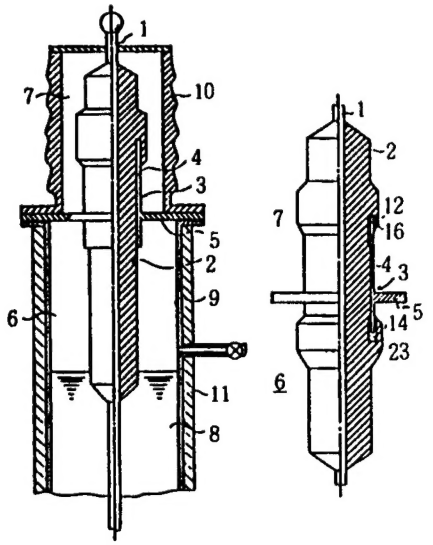

Figure 31.

Key:
1,1':	Conductor	7:	Normal temperature area
2,2':	Bushing cone	8:	Coolant
3,3':	Flange fitting	12,12':	Terminal part
4,4':	Cylinder	13,13':	Cleft
5,5':	Brim	14,14':	Terminal part
6:	Cryogenic area		

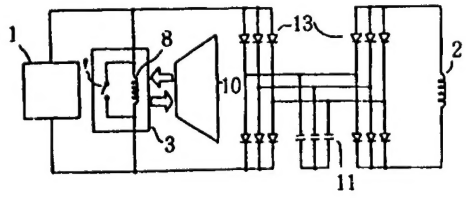

Figure 32.

Key:
1:	Solar cell array
2:	Load
3:	Chemical storage cell
4:	Diode
5,6,7,9:	Switch
8:	Superconductive electromagnet
10:	Radiating cooler
11:	Condenser
12:	Cooling system
13:	Thyristor

(7) A storage battery for use in space, having a simplified cryogenic cooler which, using a radiating cooler that takes advantage of the limitless source of low temperature (about 3 K) in outer space, cools a superconductive electromagnet capable of storing large amounts of power (Patent granted No 62-37882: NEC Corp.) (Figure 32).

5. Conclusion

This paper has described the trend of patents regarding superconductive generation of electricity (superconductive generators, MHD power generation, nuclear fusion power generation, etc.), superconductive transmission of power (DC power transmission, energy transfer, power transmission, and buried cable) and power storage systems and supply stabilization systems.

The next part will describe the trend of patents regarding magnetic resonance, superconductive sensors, superconductive elements, superconductive transistors, and superconductive computers.

References

1. Shiro Kurihara, ENERGY, Vol 4, 1988, pp 19-24.

2. Hiroshi Kaminoran, OHM, Vol 3, 1987, pp 31-35.

3. Hiroyasu Hagiwara, OYO CHODENDO, Nikkan Kogyo Shimbunsha, July 1986.

4. Takamigi Ueda, ENERGY, Vol 4, 1988, pp 30-35.

5. Toshinari Goto, CHODENDO BUSINESS, PUREJIDENTOSHA, September 1987, pp 113-148.

6. Seizo Tanaka, DENSHI JOHO TSUSHIN GAKKAISHI, Vol 2, 1988, pp 137-142.

7. Toshikatsu Tanaka, OHM, Vol 3, 1987, pp 48-52.

8. Susumu Shimamoto, Ibid., pp 54-57.

- END -

22161
45

NTIS
ATTN: PROCESS 103
BEVERLY FARRADAY
5285 PORT ROYAL RD
SPRINGFIELD, VA 22161

This is a U.S. Government publication. Its contents in no way represent the policies, views, or attitudes of the U.S. Government. Users of this publication may cite FBIS or JPRS provided they do so in a manner clearly identifying them as the secondary source.

Foreign Broadcast Information Service (FBIS) and Joint Publications Research Service (JPRS) publications contain political, economic, military, and sociological news, commentary, and other information, as well as scientific and technical data and reports. All information has been obtained from foreign radio and television broadcasts, news agency transmissions, newspapers, books, and periodicals. Items generally are processed from the first or best available source; it should not be inferred that they have been disseminated only in the medium, in the language, or to the area indicated. Items from foreign language sources are translated; those from English-language sources are transcribed, with personal and place names rendered in accordance with FBIS transliteration style.

Headlines, editorial reports, and material enclosed in brackets [ ] are supplied by FBIS/JPRS. Processing indicators such as [Text] or [Excerpts] in the first line of each item indicate how the information was processed from the original. Unfamiliar names rendered phonetically are enclosed in parentheses. Words or names preceded by a question mark and enclosed in parentheses were not clear from the original source but have been supplied as appropriate to the context. Other unattributed parenthetical notes within the body of an item originate with the source. Times within items are as given by the source. Passages in boldface or italics are as published.

SUBSCRIPTION/PROCUREMENT INFORMATION

The FBIS DAILY REPORT contains current news and information and is published Monday through Friday in eight volumes: China, East Europe, Soviet Union, East Asia, Near East & South Asia, Sub-Saharan Africa, Latin America, and West Europe. Supplements to the DAILY REPORTs may also be available periodically and will be distributed to regular DAILY REPORT subscribers. JPRS publications, which include approximately 50 regional, worldwide, and topical reports, generally contain less time-sensitive information and are published periodically.

Current DAILY REPORTs and JPRS publications are listed in *Government Reports Announcements* issued semimonthly by the National Technical Information Service (NTIS), 5285 Port Royal Road, Springfield, Virginia 22161 and the *Monthly Catalog of U.S. Government Publications* issued by the Superintendent of Documents, U.S. Government Printing Office, Washington, D.C. 20402.

The public may subscribe to either hardcover or microfiche versions of the DAILY REPORTs and JPRS publications through NTIS at the above address or by calling (703) 487-4630. Subscription rates will be provided by NTIS upon request. Subscriptions are available outside the United States from NTIS or appointed foreign dealers. New subscribers should expect a 30-day delay in receipt of the first issue.

U.S. Government offices may obtain subscriptions to the DAILY REPORTs or JPRS publications (hardcover or microfiche) at no charge through their sponsoring organizations. For additional information or assistance, call FBIS, (202) 338-6735,or write to P.O. Box 2604, Washington, D.C. 20013. Department of Defense consumers are required to submit requests through appropriate command validation channels to DIA, RTS-2C, Washington, D.C. 20301. (Telephone: (202) 373-3771, Autovon: 243-3771.)

Back issues or single copies of the DAILY REPORTs and JPRS publications are not available. Both the DAILY REPORTs and the JPRS publications are on file for public reference at the Library of Congress and at many Federal Depository Libraries. Reference copies may also be seen at many public and university libraries throughout the United States.